Modeled methanesulfonic acid (MSA) deposition in Antarctica and its relationship to sea ice

P. Hezel, B. Alexander, C. Bitz, E. Steig, C. Holmes, X. Yang, J. Sciare

Modeled methanesulfonic acid (MSA) deposition in Antarctica and its relationship to sea ice

P. J. Hezel,[1] B. Alexander,[1] C. M. Bitz,[1] E. J. Steig,[2] C. D. Holmes,[3] X. Yang,[4] and J. Sciare[5]

Received 11 June 2011; revised 22 September 2011; accepted 7 October 2011; published 15 December 2011.

[1] Methanesulfonic acid (MSA) has previously been measured in ice cores in Antarctica as a proxy for sea ice extent and Southern Hemisphere circulation. In a series of chemical transport model (GEOS-Chem) sensitivity experiments, we identify mechanisms that control the MSA concentrations recorded in ice cores. Sea ice is linked to MSA via dimethylsulfide (DMS), which is produced biologically in the surface ocean and known to be particularly concentrated in the sea ice zone. Given existing ocean surface DMS concentration data sets, the model does not demonstrate a strong relationship between sea ice and MSA deposition in Antarctica. The variability of DMS emissions associated with sea ice extent is small (11–30%) due to the small interannual variability of sea ice extent. Wind plays a role in the variability in DMS emissions, but its contribution relative to that of sea ice is strongly dependent on the assumed DMS concentrations in the sea ice zone. Atmospheric sulfur emitted as DMS from the sea ice undergoes net transport northward. Our model runs suggest that DMS emissions from the sea ice zone may account for 26–62% of MSA deposition at the Antarctic coast and 36–95% in inland Antarctica. Though our results are sensitive to model assumptions, it is clear that an improved understanding of both DMS concentrations and emissions from the sea ice zone are required to better assess the impact of sea ice variability on MSA deposition to Antarctica.

Citation: Hezel, P. J., B. Alexander, C. M. Bitz, E. J. Steig, C. D. Holmes, X. Yang, and J. Sciare (2011), Modeled methanesulfonic acid (MSA) deposition in Antarctica and its relationship to sea ice, *J. Geophys. Res.*, *116*, D23214, doi:10.1029/2011JD016383.

1. Introduction

[2] Methanesulfonic acid (MSA) concentrations in Antarctic ice cores are thought to be influenced by the distribution of nearby sea ice and have therefore been investigated with the goal of producing a proxy for sea ice cover in past climates [*Saigne and Legrand*, 1987; *Legrand and Feniet-Saigne*, 1991; *Welch et al.*, 1993; *Curran et al.*, 2003; *Abram et al.*, 2007; *Mayewski et al.*, 2009]. MSA is one of several oxidation products of dimethylsulfide (DMS), which originates in the atmosphere from biological production in the surface ocean. Observations demonstrate particularly high DMS concentrations in surface seawater in the seasonal sea ice zone around Antarctica throughout the austral spring and summer [e.g., *Kettle et al.*, 1999; *Tortell and Long*, 2009; *Gabric et al.*, 2005; *Jones et al.*, 2010]. This observed relationship constitutes the basis of the proposed link between sea ice and MSA deposition on the Antarctic continent.

[3] MSA concentrations in ice cores from various locations in Antarctica have shown inconsistent relationships with satellite observations of sea ice extent. Positive correlations of MSA with nearby sea ice extent have been reported by *Welch et al.* [1993], *Curran et al.* [2003], *Foster et al.* [2006], and *Abram et al.* [2010], with years of greater sea ice extent inducing larger areas of high DMS production and thereby increasing MSA concentrations in the ice core record. Using three ice cores from the Weddell Sea region, *Abram et al.* [2007] found negative correlations of MSA with sea ice extent in the Weddell Sea and positive correlations of MSA with sea ice extent to the west in the Bellingshausen Sea. *Pasteur et al.* [1995] and *Sun et al.* [2002] found negative correlations of MSA with sea ice extent at Dolleman Island and on the Lambert Glacier respectively.

[4] The observational literature has not yet established which processes govern MSA deposition in Antarctica and the spatial extent over which such relationships hold. In addition to sea ice, MSA concentrations have also been linked to changes in atmospheric circulation [e.g., *Becagli et al.*, 2009; *Fundel et al.*, 2006]. The extent to which MSA is

[1]Department of Atmospheric Sciences, University of Washington, Seattle, Washington, USA.
[2]Department of Earth and Space Sciences, University of Washington, Seattle, Washington, USA.
[3]Department of Earth System Science, University of California, Irvine, California, USA.
[4]NCAS-Climate, Centre for Atmospheric Science, Department of Chemistry, University of Cambridge, Cambridge, UK.
[5]LSCE, CNRS-CEA-UVSQ, Gif-sur-Yvette, France.

0148-0227/11/2011JD016383

influenced by sea ice compared to atmospheric circulation may be regionally dependent. Recent studies have questioned whether sea ice plays a significant role in measured atmospheric MSA concentrations at all. *Preunkert et al.* [2007] found that atmospheric concentrations of high DMS coincided with high MSA at Dumont D'Urville (DDU) (140°1′E, 66°40′S) on short timescales (days) and was related to simultaneous high regional chlorophyll-*a* measured by satellite, though they concluded that a relationship to sea ice was not straightforward. *Weller et al.* [2011] compared atmospheric measurements of MSA and non sea-salt sulfate ($nssSO_4^{2-}$) at Neumayer station (8°15′W, 70°39′S) and found no significant relationship between these and sea ice extent or any other climate indicators.

[5] Nearly all of the MSA-sea ice proxy studies have compared observed MSA concentrations in ice cores from point locations in Antarctica to satellite observations of sea ice extent around the continent. In this study, we use a chemical transport model to examine some of the spatial characteristics of the link between MSA and sea ice extent. The experiments were designed to understand the impact of DMS emissions from the sea ice zone on MSA deposition patterns in Antarctica, since modeling studies of the sulfur cycle have neglected this important regional source [e.g., *Cosme et al.*, 2002]. Though this sulfur source is important to understand, more fundamental characteristics of DMS emissions and MSA deposition in the high latitudes also emerge as a compelling story. In a series of model simulations with the chemical transport model GEOS-Chem [*Bey et al.*, 2001] (http://geos-chem.org), we explore the sensitivity of MSA deposition in Antarctica to modification of DMS emissions from the sea ice itself. We find that the estimates of seawater DMS emissions play a prominent role in determining whether Antarctic sulfur deposition is dominated by DMS emissions from the sea ice zone or by southward transport of sulfur emissions from lower latitudes. We fail to find credible correlations between sea ice extent and MSA deposition in Antarctica within the model given reasonable estimates of the influence of sea ice on DMS surface concentrations. Interannual variability of DMS emissions in the model, and hence interannual variability of MSA deposition, is not strongly influenced by variability in sea ice extent.

2. Model Description and Methods

2.1. Background to Model Simulations

[6] Previous global sulfur cycle modeling studies 'cap' DMS emissions in the presence of sea ice [e.g., *Chin et al.*, 2000; *Cosme et al.*, 2002], which assumes that sea ice prevents gas exchange from the ocean, even from water among sea ice floes. Though these studies broadly capture features of the Antarctic regional sulfur cycle including atmospheric concentrations, seasonal cycles, and spatial gradients in deposition fluxes [*Chin et al.*, 2000; *Cosme et al.*, 2002, 2005; *Gondwe et al.*, 2004; *Castebrunet et al.*, 2006], estimates of MSA and $nssSO_4^{2-}$ deposition to the Antarctic continent miss this important regional source. Surface seawater DMS concentrations are typically prescribed from a climatology [e.g., *Kettle et al.*, 1999; *Simó and Dachs*, 2002; *Lana et al.*, 2011], with ocean-to-air gas exchange fluxes parameterized based on empirical relationships with wind speed and SST [e.g., *Liss and Merlivat*, 1986; *Wanninkhof*, 1992; *Nightingale et al.*, 2000; *Huebert et al.*, 2010].

[7] Current understanding of both sea ice biology and gas exchange processes suggests that there may be multiple ways in which the DMS source to the atmosphere is enhanced by the presence of sea ice [*Levasseur et al.*, 1994]. Certain high DMS-producing species, including *Phaeocystis sp.*, are prevalent in Southern Ocean waters, including the sea ice zone [*Malin and Kirst*, 1997]. Melting sea ice is thought to release nutrients that stimulate a phytoplankton bloom near the ice edge [*Curran et al.*, 2003, and references therein]. Algal communities within sea ice brine pockets [*Delille et al.*, 2007] may release dimethylsulfoniopropionate (DMSP), a DMS precursor, to the water column; DMSP is then converted to DMS by enzymatic cleavage of DMSP via bacterial consumption. DMS has also been measured in pore spaces among snow crystals on sea ice [*Zemmelink et al.*, 2008], suggesting DMS may pass from ice to the atmosphere, and possibly from the water column through the ice as a result of direct gas exchange [*Gosink et al.*, 1976; *Semiletov et al.*, 2004]. Measurements of gas exchange of oxygen and sulfur hexafluoride through laboratory sea ice suggest that diffusion of gases through sea ice is much smaller than gas transfer to the atmosphere through open water leads, even when the fraction of open water is less than 1% of the ice area [*Loose et al.*, 2011].

[8] We use the GEOS-Chem model version v8-01-03 for our study, at a horizontal resolution of 2° latitude by 2.5° longitude and vertical resolution of 30 hybrid pressure-sigma levels. GEOS-Chem is a global 3-D chemical transport model [*Bey et al.*, 2001], driven by GEOS-4 meteorological fields from the Goddard Earth Observing System of the NASA Global Modeling and Assimilation Office [*Bloom et al.*, 2005]. The input meteorological fields are 3-hour averages for surface fields, 6-hour averages for upper level fields, and 6-hour instantaneous fields for sea level and surface pressures and ice extent. Meteorological fields are originally computed at a resolution of 1° latitude × 1.25° longitude, 55 vertical hybrid sigma levels, and degraded to the GEOS-Chem model resolution. We use the offline-aerosol version of GEOS-Chem, described by *Park et al.* [2004], which uses monthly mean oxidant concentrations from a full-chemistry simulation. The set of simulations are described at the end of this section, and each was begun after a 1.5 year spinup of the chemistry model.

2.2. Sea Ice and Sea Surface Temperature

[9] Sea ice extent and sea surface temperature (SST) are specified from NOAA Optimum Interpolation (OI v.2) weekly fields [*Reynolds et al.*, 2002], interpolated to 6-hour instantaneous fields at 1° × 1° resolution. Sea ice in GEOS-Chem is a binary field (the ocean fraction of a grid cell is either all ice or ice free) on the model grid. When the OI v.2 is degraded to 2° × 2.5° resolution, a grid cell is designated 'ice' if more than 50% of the area is covered with ice concentration of 15% or greater.

2.3. Ocean-to-Air DMS Emissions and Surface Seawater DMS Concentrations

[10] Atmospheric DMS emissions from seawater are parameterized using a climatology of surface seawater DMS concentrations [*Simó and Dachs*, 2002; *Kettle et al.*, 1999;

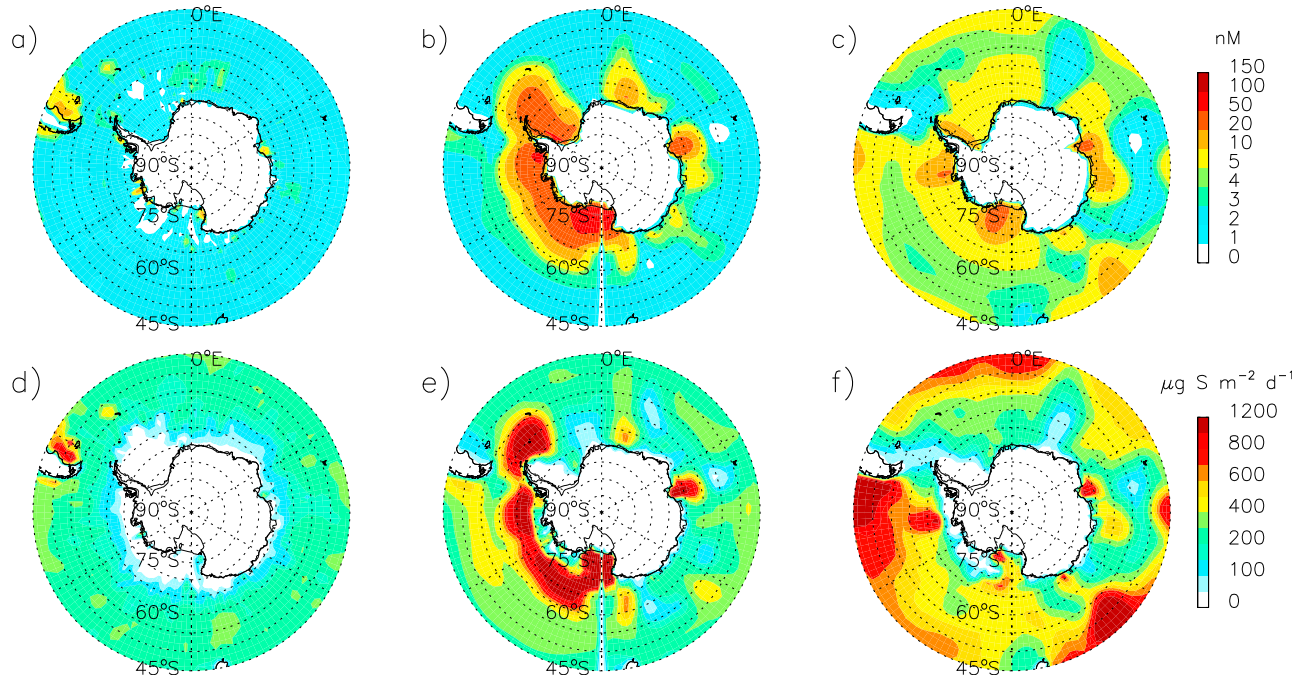

Figure 1. January surface DMS concentrations (nM) from (a) *Simó and Dachs* [2002], (b) *Kettle et al.* [1999], and (c) *Lana et al.* [2011] DMS data sets. January climatological DMS emissions fluxes (μg m^{-2} d^{-1}) in the (d) Simó and Dachs 'capped', (e) Kettle1999 'capped', and (f) Lana 2011 'capped' simulations, where DMS emissions fluxes are zero in the presence of sea ice. Scales are not linear. See section 2.8 and Table 1 for the description of the simulations.

Lana et al., 2011] combined with a sea-to-air transfer velocity computed as a function of instantaneous 10-meter wind speed and SST [*Nightingale et al.*, 2000; *Huebert et al.*, 2010].

[11] The *Nightingale et al.* [2000] parameterization is used primarily in our simulations and specifies a quadratic dependence on wind speed, which implies more efficient gas transfer at higher wind speeds than the linear dependence specified in the widely-used *Liss and Merlivat* [1986] parameterization. Recent measurements, however, suggest that the DMS sea-to-air transfer velocity at medium wind speeds (4–12 m s^{-1}) is at best described by a linear dependence on wind speeds [*Huebert et al.*, 2010]. A sensitivity test using the *Huebert et al.* [2010] parameterization shows that our results are not strongly dependent on the difference between these parameterizations.

[12] The three DMS climatologies used in this study are from *Simó and Dachs* [2002], *Kettle et al.* [1999], and *Lana et al.* [2011]. All three originate from a compilation of *in situ* surface seawater DMS concentration measurements in the Global Surface Seawater DMS Database (GSSDD, http://saga.pmel.noaa.gov/dms) begun following the publication of the climatology by *Kettle et al.* [1999]. We primarily use DMS concentrations from a monthly climatology following *Simó and Dachs* [2002], and present results using the other two [*Kettle et al.*, 1999; *Lana et al.*, 2011] in sensitivity studies. *Simó and Dachs* [2002] determined an empirical relationship between the seawater DMS concentrations in the GSSDD and simultaneous measurements of chlorophyll-a (Chl-*a*) concentrations at the surface and the mixed layer depth (MLD). A global DMS data set is then derived from global data sets of Chl-*a* and MLD. We use a *Simó and Dachs* [2002] DMS climatology derived from Chl-*a* estimates from the Sea-viewing Wide Field-of-view Sensor (SeaWiFS) monthly climatological data from 2001–2006 and ocean MLD monthly climatology from *de Boyer-Montegut et al.* [2004]. The widely-used *Kettle et al.* [1999] DMS data set interpolates the GSSDD measurements into a monthly climatology. The *Lana et al.* [2011] DMS climatology was constructed using the three-fold increase in GSSDD measurements over *Kettle et al.* [1999] projected onto biogeographic provinces and processed with objective techniques to obtain monthly fields.

[13] Since SeaWiFS data do not provide reliable Chl-*a* estimates in areas with sea ice, persistent cloud cover or during the polar night, the *Simó and Dachs* [2002] DMS data set does not report high latitude DMS concentrations under extensive ice or cloud conditions. We replace missing DMS concentrations in the Southern Ocean using an average of concentrations immediately to the north of the missing data. This simple fix enables the spatial continuity of DMS emissions in the Southern Ocean without the additional impact of missing concentration values in the sea ice zone. High latitude DMS concentrations in the *Simó and Dachs* [2002] DMS data set are below the peak *in situ* measurements in the GSSDD and hence are likely a lower bound on the true concentration fields in the sea ice zone under extensive ice coverage.

[14] Figure 1 shows the January surface seawater DMS concentrations from the *Simó and Dachs* [2002], *Kettle et al.* [1999], and *Lana et al.* [2011] DMS data sets and the corresponding mean DMS emission fluxes to the atmosphere

from our simulations using the *Nightingale et al.* [2000] parameterization. The interpolation of sparse spatial and temporal *in situ* DMS measurements in the *Kettle et al.* [1999] data set results in extensive hot-spots and strong zonal gradients in DMS concentrations and emissions within the sea ice zone. We use the *Simó and Dachs* [2002] DMS climatology in our primary simulations because it lacks this strong zonal asymmetry in DMS concentrations.

[15] Global DMS surface concentrations are difficult to estimate from present measurements, as seen in the wide variation of DMS concentrations and resulting emissions in Figure 1. Ecological and biogeochemical dynamics within planktonic communities also play a significant role in determining DMS production and hence DMS emissions [*Elliott*, 2009; *Cameron-Smith et al.*, 2011]; these dynamics are not represented in the DMS seawater climatologies used in our model simulations. The use of a surface seawater DMS concentration climatology in the model neglects any interannual variability in surface DMS concentrations, though the interannual variability of DMS emissions is approximated to some extent via the interannual variability in SSTs and winds that govern the DMS ocean-to-air flux parameterizations.

2.4. Other Sulfur Emissions

[16] Natural (except DMS), anthropogenic, and biomass burning sulfur emissions are from the Global Emissions Inventory Activity (GEIA v.1) database (http://www.geiacenter.org/). Non-DMS emissions in all simulation years are prescribed at 1995 magnitudes to restrict interannual sulfur cycle variability to processes associated with DMS. Volcanic emissions are included in the GEIA as part of the natural source emissions, and include an average of continuous volcanic emissions over 25 years plus eruptive volcanic emissions. Ship SO_2 emissions follow *Corbett et al.* [1999]. The model does not include sea-salt sulfate emissions, and therefore all sulfate in the model is non-sea-salt sulfate ($nssSO_4^{2-}$).

2.5. DMS Chemistry

[17] The oxidative pathways of DMS are complex and not completely understood [*von Glasow and Crutzen*, 2004; *Lucas and Prinn*, 2005] and typically are simplified in large scale models. [e.g., *Chin et al.*, 1996; *Cosme et al.*, 2002]. DMS is thought to be oxidized in the atmosphere to SO_2 and MSA primarily by the hydroxyl radical (OH) and the nitrate radical (NO_3). Measurements of BrO have been shown to be high in the presence of first-year sea ice [*Wagner et al.*, 2007; *Alvarez-Aviles et al.*, 2008; *Simpson et al.*, 2007], and halogen (BrO) chemistry is also known to play a role in DMS oxidation [*Boucher et al.*, 2003; *Read et al.*, 2008]. The magnitude, variability, and relative importance of BrO is not yet well understood. SO_2 is further oxidized to sulfate and contributes the dominant fraction of $nssSO_4^{2-}$ aerosols in remote marine locations. Sulfate has other natural and anthropogenic origins which confound its relationship to DMS, but it is thought that MSA is a product only of DMS oxidation. In a study of seven DMS oxidation schemes, *Karl et al.* [2007] showed that the relatively simple DMS chemistry used by *Chin et al.* [1996] (and used in this study) reproduced observed features of the sulfur cycle extremely well compared to more complicated mechanisms.

[18] The DMS-MSA chemistry in GEOS-Chem is simplified as described by *Chin et al.* [1996, 2000]. Yields for DMS oxidation via gas-phase reaction with OH are 100% SO_2 (abstraction channel) and 75% SO_2 and 25% MSA (addition channel). The fraction of DMS oxidized to MSA is larger in the high latitudes than globally, due to the temperature dependence of the OH reaction. DMS reaction with NO_3 in the gas phase also yields 100% SO_2, however reaction with NO_3 is limited to periods of no solar insolation. Globally, 26% of DMS oxidation occurs via reaction with NO_3.

[19] Gas phase DMS oxidation by BrO produces dimethylsulfoxide (DMSO) which is further oxidized in the gas phase to MSA [*Breider et al.*, 2010]. A simplified BrO oxidation mechanism was added in a sensitivity study as:

$$\mathrm{DMS} + \mathrm{BrO} \rightarrow 0.6 \cdot \mathrm{SO_2} + 0.4 \cdot \mathrm{MSA} \quad (1)$$

[*Pham et al.*, 1995; *Boucher et al.*, 2002; *Chatfield and Crutzen*, 1990; *Breider et al.*, 2010] using a pseudo-first order rate constant of $k = 1.5 \times 10^{-14} \exp(1000/T)$[BrO] [*IUPAC*, 2007]. This reaction assumes all DMS is oxidized to SO_2 and MSA and neglects the intermediate product dimethylsulfoxide (DMSO) and its deposition, since DMSO is not explicitly included in the current model. This simplified chemistry will lead to an overestimate of MSA produced via DMS oxidation by BrO. A simple diurnal cycle was imposed by setting the rate constant to zero in the absence of sunlight.

2.6. Aerosol Deposition

[20] Wet deposition of aerosols is described by *Liu et al.* [2001] and includes contributions from scavenging in convective updrafts, rainout and washout from convective anvils and large scale precipitation, and return to the atmosphere following re-evaporation. Dry deposition velocities are computed with a standard resistance-in-series scheme based on work by *Wesely* [1989] as described by *Wang et al.* [1998]. Since deposition processes on Antarctica occur primarily on snow surfaces for both dry and wet deposition, sulfate deposition is calculated as the sum of both SO_2 and sulfate for both wet and dry processes. Snow concentrations of MSA and other species are computed as $\frac{F_i}{p}$, where F_i is the monthly mean deposition flux of chemical tracer i (kg m^{-2} d^{-1}), and p is the monthly mean precipitation (mm d^{-1}). Seasonal and yearly averages of MSA snow concentration are computed as precipitation-weighted means.

2.7. Meteorology

[21] Figure 2 shows GEOS-4 annual precipitation (mm yr^{-1} water equivalent) in Antarctica with maximum values (400–1000 mm yr^{-1}) at the coast decreasing inland (10–100 mm yr^{-1}). Comparison of GEOS-4 precipitation rates for Antarctica with those from *Monaghan et al.* [2006] reveal no significant bias. *Monaghan et al.* [2006] derived a 50-year time series of snowfall accumulation over Antarctica by combining model simulations and observations primarily from ice cores. *Bloom et al.* [2005] evaluated the GEOS-4 analysis data set compared to observations and other reanalysis products and note an underestimation by up to a factor of two in precipitation of the Southern Hemisphere

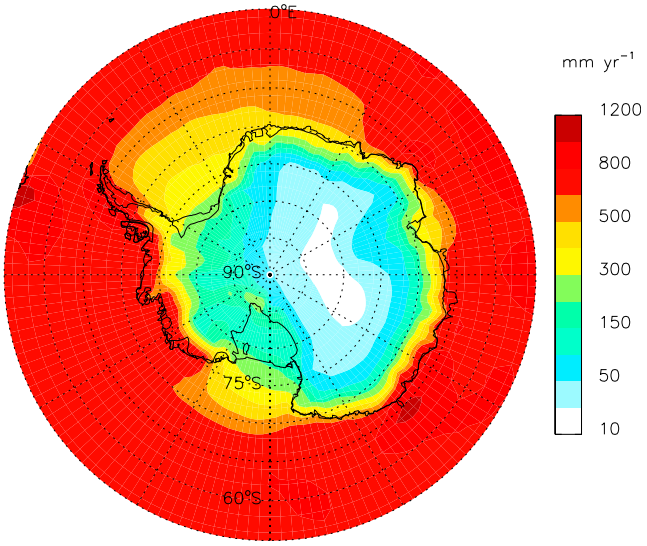

Figure 2. Mean annual precipitation rate (mm yr^{-1} water equivalent) from GEOS-4 meteorological fields.

extratropics (30–60°S) and a high bias in zonal austral summer winds in the Southern Ocean (40–60°S).

[22] We also conduct a sensitivity study with GEOS-5 meteorology data, which has higher boundary layer resolution than GEOS-4. We examine whether the reduced boundary layer resolution of GEOS-4 overestimates transport out of the boundary layer into the free troposphere. GEOS-5 also corrects some of the low bias in precipitation in the Southern Ocean, with increases of 25–100% over GEOS-4 precipitation in the 30–60°S region. Antarctic continental precipitation, however, is lower in GEOS-5 compared to GEOS-4. In most locations in Antarctica precipitation is within 25% of GEOS-4 values, though in some sections of West Antarctica precipitation is lower by 50% in the GEOS-5 data. The effects of the GEOS-5 meteorology on our simulations are discussed in detail in section 4.7, but the sensitivity study indicates that the choice of meteorological input does not change our conclusions. We use the GEOS-4 meteorology for our primary simulations because of the longer time period over which meteorological data is available for GEOS-Chem (1985–2006 for GEOS-4, compared to 2004-present for GEOS-5).

2.8. Simulations

[23] As in most sulfur models, GEOS-Chem implements a 'cap' associated with gas exchange through the sea ice, and therefore assumes that DMS emissions are zero within the sea ice by default. We experiment with relaxing this condition in our scenarios, whereby we use the same gas transfer parameterization over sea ice as over open ocean. We assume that the gas transfer parameterization over sea ice is appropriate for the sea ice fraction as well as open water among sea ice floes, which may not be realistic [e.g., *Loose et al.*, 2011]. This is, however, useful as a first order determination of the influence of DMS emissions from within the sea ice itself. In three model scenarios we vary the DMS concentrations in the presence of sea ice from October through March. The 'capped' scenario uses this default cap on DMS emissions in the presence of sea ice in all months. The 'uncapped' scenario removes the cap from October through March, effectively removing the influence of sea ice on DMS fluxes from the ocean except via the influence of sea ice on SST. A third scenario is an 'enhanced' run where the surface DMS concentration is set to 6 nM wherever sea ice is

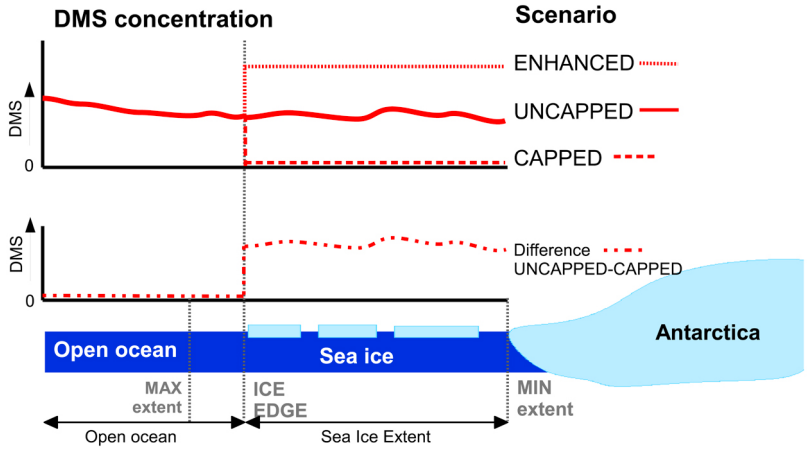

Figure 3. Illustration of seawater DMS concentrations applied in the sea ice zone for each of the scenarios. (top) DMS concentrations for the DMS data set are applied to the open ocean and the sea ice in the UNCAPPED scenario (solid red line), with no influence of sea ice. For the CAPPED scenario, DMS concentrations are set to 0 (dashed red line). In the ENHANCED scenario, DMS concentrations are set to a scalar value above the mean DMS concentrations of the ice extent (fine dashed red line). (bottom) The difference (UNCAPPED minus CAPPED) between two scenarios allows evaluation of effect of DMS concentrations of the DMS data set from within sea ice only (red dot-dot-dashed line). In all simulations, the sea ice expands and retreats through its seasonal cycle (between maximum and minimum ice extent). Each scenario is applied for the to the sea ice extent at each point in time for the months October–March. All simulations have a 'capped' scenario for April–September.

Table 1. Summary of Simulations and Sensitivity Simulations Discussed in the Text

Simulation Name	DMS Conc in Ice	DMS Emissions		Simulation Length	Sensitivity Test
		DMS Data Set[a]	Parameterization[a]		
Simó and Dachs capped	0	SD2002	N2000	17 years (7/1985-6/2004)[b]	
Simó and Dachs uncapped	Oct-Mar: Data set; Apr-Sep: 0	SD2002	N2000	17 years (7/1985-6/2004)[b]	
Simó and Dachs enhanced	Oct–Mar: 6 nM; Apr–Sep: 0	SD2002	N2000	17 years (7/1985–6/2004)[b]	
Huebert2010 capped	0	SD2002	H2010	3 yrs (7/1985–6/1988)	Emissions linear with wind speed
Huebert2010 uncapped	Oct–Mar: Data set; Apr–Sep: 0	SD2002	H2010	3 yrs (7/1985–6/1988)	Emissions linear with wind speed
BrO capped	0	SD2002	N2000	3 yrs (7/1985–6/1988)	BrO oxidation mechanism
BrO uncapped	Oct-Mar: Data set; Apr-Sep: 0	SD2002	N2000	3 yrs (7/1985–6/1988)	BrO oxidation mechanism
GEOS-5 capped	0	SD2002	N2000	2 yrs (7/2005–6/2007)	GEOS-5 meteorological data set
GEOS-5 uncapped	Oct-Mar: Data set; Apr-Sep: 0	SD2002	N2000	2 yrs (7/2005-6/2007)	GEOS-5 meteorological data set
Kettle1999 capped	0	K1999	N2000	6 yrs (7/1985–6/1991)	Alternate DMS data set
Kettle1999 uncapped	Nov–Mar: Data set; Apr–Oct: 0	K1999	N2000	6 yrs (7/1985–6/1991)	Alternate DMS data set
Lana2011 capped	0	L2011	N2000	3 yrs (7/1985–6/1988)	Alt. DMS data set emissions only
Lana2011 uncapped	Oct–Mar: Data set; Apr–Sept: 0	L2011	N2000	3 yrs (7/1985–6/1988)	Alt. DMS data set emissions only

[a]Abbreviations: SD2002, *Simó and Dachs* [2002]; N2000, *Nightingale et al.* [2000]; H2010, *Huebert et al.* [2010]; K1999, *Kettle et al.* [1999]; L2011, *Lana et al.* [2011].

[b]Data from July 1997–June 1999 was excluded from the analysis because of an error in regridding GEOS-4 surface precipitation and specific humidity tendency fields for GEOS-Chem.

present from October through March. Figure 3 illustrates the DMS concentrations imposed in the sea ice in each of these scenarios. We also examine the difference between the uncapped and capped runs to examine the impact of DMS emissions only from within the sea ice.

[24] Table 1 summarizes all simulations discussed in the paper. Our primary simulations use the *Simó and Dachs* [2002] DMS climatology with the *Nightingale et al.* [2000] gas transfer parameterization under the capped, uncapped, and enhanced scenarios as described above. These are referred to in the text below as 'Simó and Dachs capped', 'Simó and Dachs uncapped', etc. The *Simó and Dachs* [2002] DMS data set has a mean DMS concentration from October-March over the climatological sea ice area of 1.2 nM, with a peak concentration of 2.0 nM in January. The 6 nM concentration is thus 5 times larger than the October-March mean of the uncapped run. We compute the difference between the uncapped and capped and the enhanced and capped model scenarios to isolate the effect of DMS emissions from within sea ice itself. The Simó and Dachs capped, uncapped, and enhanced simulations are run for 17 years from July 1985 through June 2004 after a 1.5 year spin up, excluding the period July 1997 through June 1999. This overlaps the period of satellite observations of sea ice as well as several ice core records of MSA concentrations.

[25] To determine appropriate DMS concentrations to use in sea ice in the enhanced simulation, we consulted DMS surface concentration measurements from the Global Surface Seawater DMS Database. When averaged into monthly 5° zonal bands between 60°S and 75°S, monthly median concentrations in each band range between 1–7 nM over the course of the austral summer. Regions of very high median DMS concentration (>10 nM) in the Weddell and Ross Seas near their respective ice shelves were excluded. Though the observed monthly median values exhibit a seasonal cycle, a constant value of 6 nM was prescribed in the enhanced simulation for October through March. These prescribed concentrations are low compared to the range of DMS seawater measurements associated with the seasonal sea ice zone [e.g., *Jones et al.*, 2010], but they are enhanced compared to the mean values contained in the *Simó and Dachs* [2002] DMS data set as noted above, and are therefore useful in evaluating the sensitivity of MSA deposition to DMS emissions from the sea ice itself. In the capped run, over 56% and up to 90% of the annual MSA deposited at each spatial location in Antarctica occurs between October and March, forming the basis of the seasonality in modified DMS concentrations.

[26] In addition to the 17-year Simó and Dachs simulations described above, several other sensitivity runs were completed to examine our results with different DMS concentrations and gas flux parameterizations (see Table 1). Simulations using the *Kettle et al.* [1999] DMS data set and the *Nightingale et al.* [2000] emissions parameterization were each run for six years to understand the sensitivity of our results to the specific DMS concentration data set (Kettle1999 capped and Kettle1999 uncapped). The sensitivity of our results to the DMS flux parameterization was investigated using the *Huebert et al.* [2010] parameterization, which describes a linear function of DMS emissions with wind speed (Huebert2010 capped and Huebert2010 uncapped). A BrO sensitivity study was conducted by implementing a simplified BrO oxidation mechanism (described in section 2.5) and utilizing monthly mean BrO fields from *Holmes et al.* [2010] and *Yang et al.* [2005] (BrO capped and BrO uncapped). The BrO sensitivity study includes capped and uncapped simulations using the *Simó and Dachs* [2002] surface ocean DMS concentrations and the *Nightingale et al.* [2000] gas transfer parameterization. A sensitivity experiment was performed using the GEOS-5 meteorological data in order to investigate the dependence of our results on the boundary layer resolution and other meteorological input fields (GEOS-5 capped and GEOS-5 uncapped). Finally, the *Lana et al.* [2011] DMS surface seawater climatology was used to estimate the set of both capped and uncapped DMS emissions using the *Nightingale et al.* [2000] gas transfer parameterization and the GEOS-4 meteorology fields (Lana2011 capped and Lana2011 uncapped). We find that

Table 2. Annual Global Sulfur Budget for Simó and Dachs Capped Run Compared to Global Sulfur Budgets Summarized in Other Studies[a]

	Capped Run Mean ± 1σ	Published Range Min - Max
Total Sulfur Emissions (Tg S y^{-1})	97.3 ± 0.8	83–124.6[b]
DMS oceanic emissions	23.6 ± 0.9	10.7–27.9[c]
Total Sulfur Deposition (Tg S y^{-1})	95.2 ± 0.7	82.3–95.6[d]
SO_2 dry deposition	30.7 ± 0.4	23–55[b]
SO_2 wet deposition	14.9 ± 0.3	0.2–19.9[b]
Sulfate dry deposition	6.0 ± 0.1	3.2–17[c]
Sulfate wet deposition	41.5 ± 0.8	24.7–74.1[c]
MSA dry deposition	0.2 ± 0.0	
MSA wet deposition	1.9 ± 0.1	
Burden (Tg S)		
SO_2	0.36 ± 0.00	0.2–0.68[b]
Sulfate	0.60 ± 0.01	0.5–0.96[d]
DMS	0.11 ± 0.00	0.02–0.15[b]
MSA	0.04 ± 0.00	0.02–0.03[b]
Lifetime (days)		
SO_2	1.46 ± 0.02	0.6–5.3[b]
Sulfate	4.66 ± 0.12	3.4–7.2[c]
DMS	1.77 ± 0.04	0.5–3[b]
MSA	6.71 ± 0.35	5.6–18.5[b]

[a]Uncertainties are one standard deviation of annual global means over 17 years of simulation.
[b]Summarized by *Faloona* [2009].
[c]Summarized by *Spracklen et al.* [2005].
[d]Summarized by *Berglen et al.* [2004].

emissions using the *Simó and Dachs* [2002] and *Kettle et al.* [1999] DMS data sets bracket DMS emissions obtained using *Lana et al.* [2011], and results of a chemistry simulation with the *Lana et al.* [2011] DMS climatology would yield little new information to our analysis here.

3. Model Evaluation

3.1. Global Sulfur Budget

[27] Table 2 compares the annual global sulfur budget for the capped simulation with other published estimates of the global sulfur cycle. Annual DMS emissions of 23.6 Tg S yr^{-1} using the *Simó and Dachs* [2002] DMS data set and the *Nightingale et al.* [2000] emissions parameterization are within the range of estimates of 10–40 Tg S y^{-1} summarized by *Penner et al.* [2001]. We note that the *Simó and Dachs* [2002] DMS data set results in larger global DMS emissions than both the *Kettle et al.* [1999] DMS data set (19.6 Tg S y^{-1}) and the *Lana et al.* [2011] DMS data set (22.2 Tg S y^{-1}) under a capped sea ice emissions scenario. Global DMS emissions are larger in our simulations than estimates made with the widely-used *Liss and Merlivat* [1986] parameterization for sea-to-air flux [*Kettle and Andreae*, 2000; *Nightingale et al.*, 2000], as a result of the greater sensitivity to higher wind speeds in the Nightingale parameterization. Lifetimes are calculated as mean burden divided by the sum of the loss processes (i.e., chemical loss for lifetimes of DMS, and deposition for MSA). Global annual lifetimes of DMS and MSA are 1.8 and 6.7 days for the capped run. These estimates are comparable to other published estimates of the lifetime of both MSA and DMS [e.g., *Faloona*, 2009; *Spracklen et al.*, 2005; *Berglen et al.*, 2004; *Chin et al.*, 2000]. Global budgets of SO_2 and SO_4^{2-} also compare well to previously published estimates.

[28] Emissions of DMS from within sea ice have only a modest effect on the global sulfur budget, and 'capping' emissions in the presence of sea ice has likely been appropriate in studies of the global sulfur cycle. The increases in global sulfur emissions in the Simó and Dachs uncapped and enhanced DMS runs over the capped run are 0.05 Tg S y^{-1} (<1%) and 0.31 Tg S y^{-1} (1.4%) respectively; these increases are less than the magnitude of interannual variability of global DMS emissions (~1 Tg S y^{-1}) caused by variability in wind speeds and SSTs. The increase in global DMS emissions in the Kettle1999 uncapped run compared to the capped run is also small (0.36 Tg S y^{-1}, or 1.8%).

3.2. Comparison of Modeled and Observed Atmospheric Concentrations

[29] We compared the modeled atmospheric concentrations of MSA, $nssSO_4^{2-}$, and DMS at Antarctic locations where observational data exist. Figure 4 shows modeled monthly mean concentrations of MSA, $nssSO_4^{2-}$ and DMS at Dumont D'Urville (DDU) (140°1′E, 66°40′S) compared to observations [*Minikin et al.*, 1998; *Preunkert et al.*, 2008]. The modeled and observed high-latitude atmospheric MSA and $nssSO_4^{2-}$ concentrations at the surface exhibit a maximum in austral summer and minimum in austral winter (Figures 4a and 4b). The seasonal maximum in MSA is broad in both observations and the model, showing high MSA values (16–18 ppt) lasting from late summer through autumn. The winter minimum (2–3 ppt), however, is shorter in the model than in observations, with modeled concentrations increasing earlier (in August) than observations after the winter minimum. The Kettle1999 capped simulation overestimates the summer MSA maximum by a factor of 3 and does not capture the late summer peak, but better simulates the timing of the rise in concentrations after summer and into the spring season than the Simó and Dachs capped simulation. Modeled $nssSO_4^{2-}$ concentrations match the observations at DDU well, capturing both the magnitude and timing of the seasonal cycle through both the summer and winter (Figure 4b). The Kettle1999 capped simulation overestimates the magnitude of the $nssSO_4^{2-}$ summer peak but captures the winter minimum quite well. *Kettle and Andreae* [2000] corrected some of the errors associated with the DMS concentrations at high latitudes in the *Kettle et al.* [1999] DMS data set that lead to the very large austral summer peaks in MSA and $nssSO_4^{2-}$.

[30] Similar characteristics are found in comparisons of modeled MSA and $nssSO_4^{2-}$ to station observations for Halley (26°19′W, 75°35′S), Mawson (62°30′E, 67°36′S), Neumayer (8°15′W, 70°39′S), and Palmer stations (64°03′W, 64°46′S) (not shown) [*Minikin et al.*, 1998; *Savoie et al.*, 1993]. In all cases, the comparison of modeled MSA and $nssSO_4^{2-}$ to observations is similar to that at DDU. Modeled MSA concentrations increase earlier in springtime (August) than in observations, reach summer maxima in February-March, and overestimate winter minima.

[31] Figure 4c shows surface DMS concentrations at DDU in the model compared to observations [*Preunkert et al.*, 2008]. Modeled summer values at DDU show reasonable agreement with observations (within a factor of 3), but winter values are substantially overestimated. The buildup of

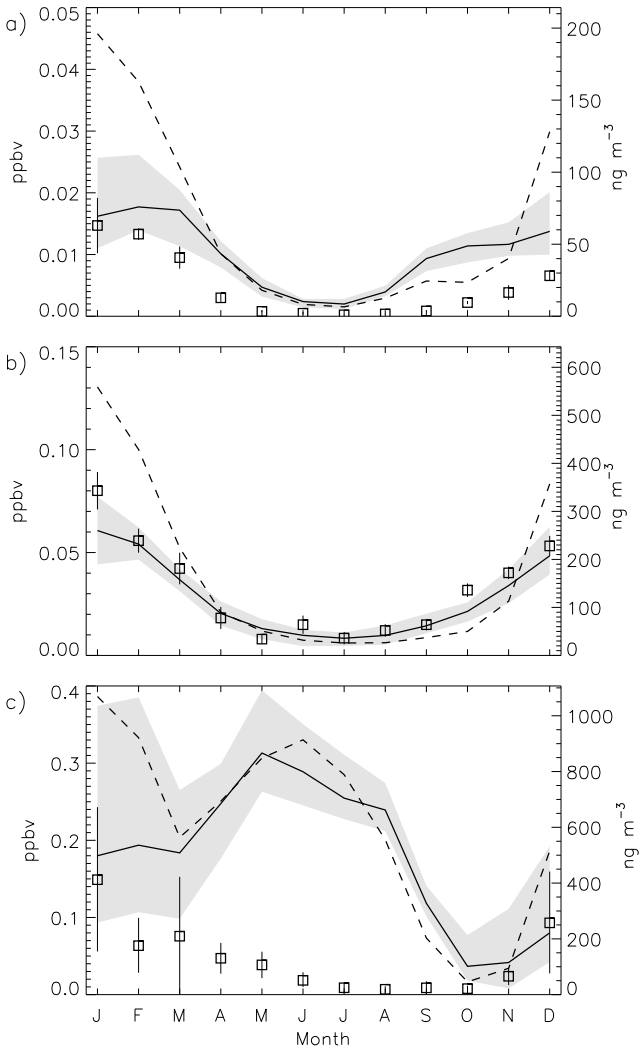

Figure 4. Annual cycle of (a) MSA concentrations (ppb), (b) nssSO_4^{2-} concentrations (ppb), and (c) DMS concentrations (ppb) at the surface at Dumont D'Urville (140°1′E, 66°40′S). The monthly mean (solid line) and minima/maxima (shaded) for the Simó and Dachs capped simulation from the 17 year run are shown with the Kettle1999 capped monthly mean for the 6 year run (dashed line). Observations are shown as open squares with the standard deviation as reported by *Preunkert et al.* [2008] and *Minikin et al.* [1998].

DMS in the high latitudes in the austral winter is related to the lack of a chemical sink in the model, due to the lack of a local source of NO_x (leading to low NO_3) and the lack of available sunlight (leading to low OH). Owing to the low solubility of DMS, its depositional sink is insignificant, even in winter.

[32] Gas- and aqueous-phase oxidation of DMS by O_3, not included in GEOS-Chem, has been shown by *Boucher et al.* [2003] to be important in the high latitudes. Aqueous and gas phase oxidation of DMS by O_3 has been estimated to account for 30–40% of the annual DMS oxidation over the Southern Ocean and Antarctica though it contributes only up to 6% of oxidation of DMS globally. Though no seasonal figures are shown by *Boucher et al.* [2003], gas- and aqueous-phase DMS oxidation by O_3 contributes little to DMS oxidation at low and mid latitudes, and therefore likely contributes little in the high latitude austral summer when OH and NO_3 dominate DMS oxidation. This suggests that oxidation by gas- and aqueous-phase O_3 dominates in the high latitude austral winter due to the lack of other oxidants. *Barnes et al.* [2006] outlines an argument for the importance of this oxidation pathway in global sulfur models, and its absence likely explains the discrepancy in the modeled seasonality of atmospheric DMS concentrations at high southern latitudes.

[33] Our analysis of model results is restricted to the austral spring and summer months of October-March, and therefore the high winter bias in atmospheric concentrations of both DMS and MSA at high latitude stations has little impact on our results. The lifetimes of both DMS and MSA are relatively short (4.7 and 10.9 days for DMS and MSA calculated for September-November) in the early spring south of 60°S, and therefore the high winter DMS concentrations have little effect on October-March MSA deposition. Modeled October-March DMS and MSA atmospheric concentrations agree with the observations within a factor of 2 and 3 respectively.

[34] We also compared the model to observations of atmospheric DMS at the lower-latitude stations of Cape Grim (144°41′E, 40°41′S) and Amsterdam Island (77°30′E, 37°50′S), shown in Figure 5 [*Ayers et al.*, 1995; *Sciare et al.*,

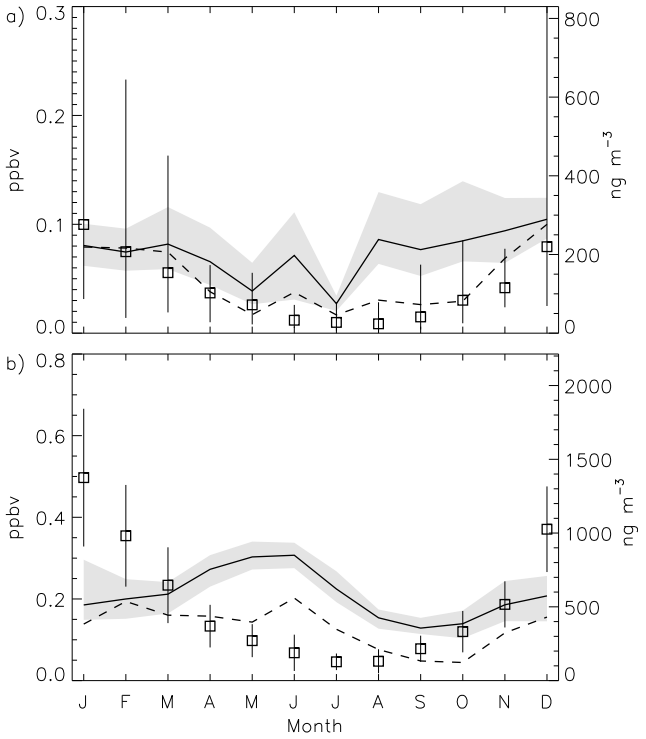

Figure 5. Annual cycle of DMS concentrations (ppb) at the surface at (a) Cape Grim (144°41′E, 40°41′S) and (b) Amsterdam Island (77°30′E, 37°50′S). Lines and symbols are the same as in Figure 4. Observations for Cape Grim are from *Ayers et al.* [1995]; error bars indicate the spread of measurements from *Ayers et al.* [1995, Figure 3]. Observations from Amsterdam Island cover the period 1987–2010 following the protocols reported by *Sciare et al.* [2000]. Error bars indicate the standard deviation in monthly means.

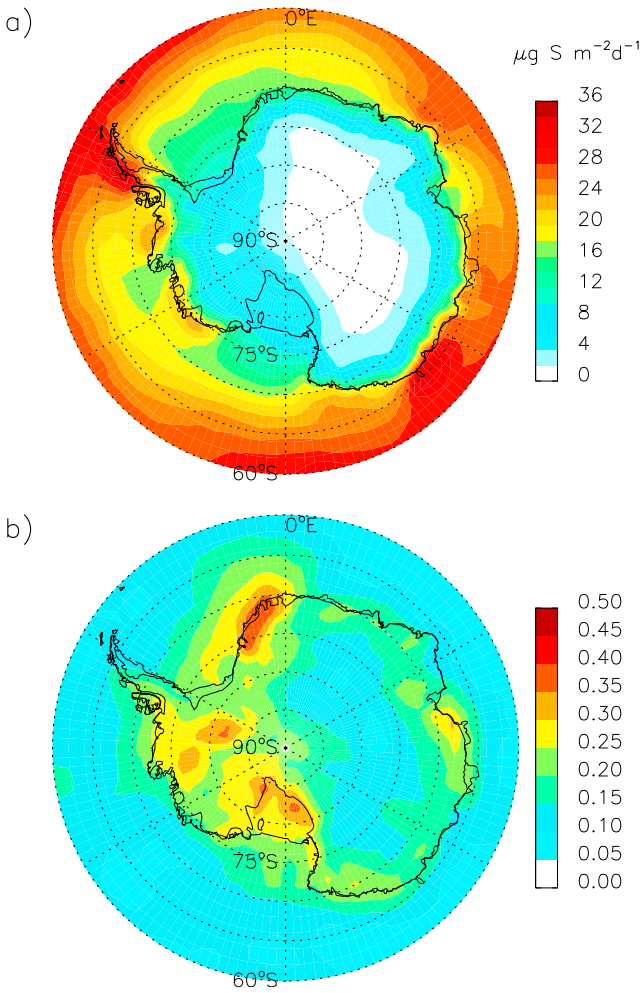

Figure 6. (a) Mean MSA deposition flux (μg S m^{-2} d^{-1}) for October-March from the capped run. (b) Standard deviation (unitless) of MSA deposition flux, normalized by Figure 6a.

2000]. Observations at both of these sites show a clear austral summer maximum and winter minimum. There is no clear seasonal cycle in the model at Cape Grim in the Simó and Dachs capped simulation owing to the lack of seasonal cycle in the DMS emissions from the *Simó and Dachs* [2002] DMS data set. The Kettle1999 capped simulation captures the observed seasonal cycle reasonably well, which reflects the seasonal cycle in modeled DMS emissions in that region. At Amsterdam Island, neither DMS climatology results in the capture of the observed seasonal cycle, which again reflects local model DMS emissions. This comparison of Cape Grim and Amsterdam Island illustrates that the atmospheric DMS concentrations depend strongly on the seawater DMS climatology. A comprehensive set of measurements of DMS seawater concentration, DMS emissions, and DMS and MSA surface air concentration would be extremely valuable for further assessing the model, even if only at a few locations.

3.3. Mean MSA Deposition Fluxes and Snow Concentrations

[35] Figure 6 shows the 17-year mean MSA deposition flux from October-March near Antarctica for the Simó and Dachs capped run. Modeled mean MSA deposition fluxes exhibit a strong gradient from the coast decreasing inland in Antarctica, similar to the gradient shown in the mean annual precipitation in Figure 2. MSA deposition fluxes are dominated by wet deposition processes at locations covering 82% of the Antarctic land area, and MSA deposition fluxes are strongly correlated with precipitation ($r^2 = 0.78$) in the Simó and Dachs capped run in Antarctica.

[36] Figure 7 shows the 17-year mean MSA snow concentration from October-March in Antarctica, compared to spring, summer, and annual measurements of MSA concentrations in ice cores and snow pits compiled from 520 sites by *Bertler et al.* [2005]. Modeled snow concentrations of MSA are of the same order of magnitude as measured snow pit and ice core measurements, though on average they are overestimated in the model by up to a factor of 5 at the coasts in the modeled annual mean concentrations. Snow

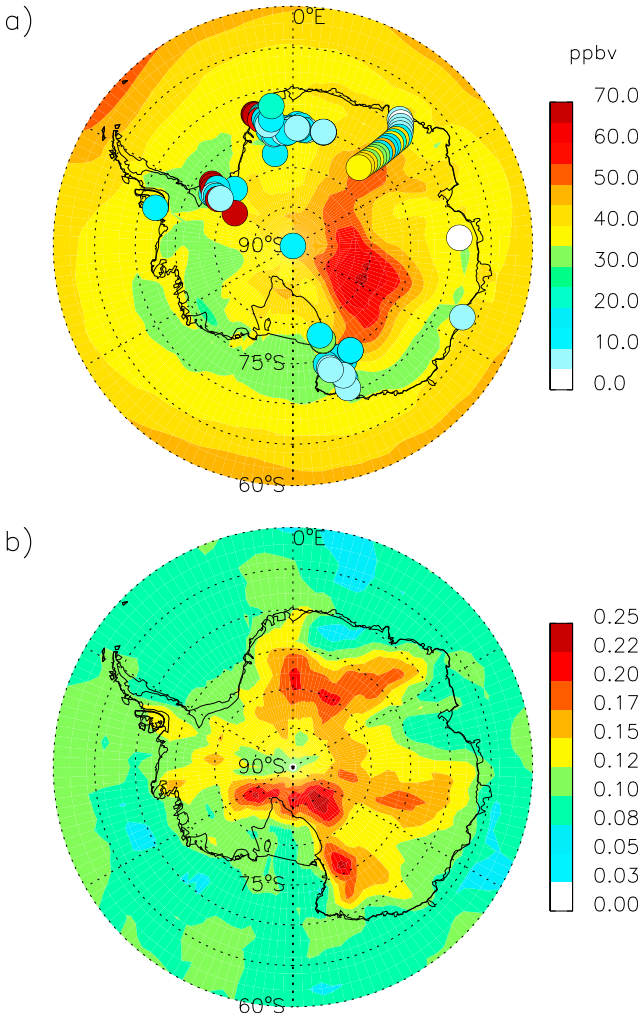

Figure 7. (a) Mean MSA snow concentration (ppb) for October-March from the capped run. Filled circles are MSA concentration measurements compiled from snow and ice chemistry at 520 sites across Antarctica by *Bertler et al.* [2005]. (b) Normalized standard deviation of MSA snow concentration (unitless). Values are displayed over the ocean as well as land to understand the spatial patterns, even though rainfall/snowfall does not accumulate over the ocean.

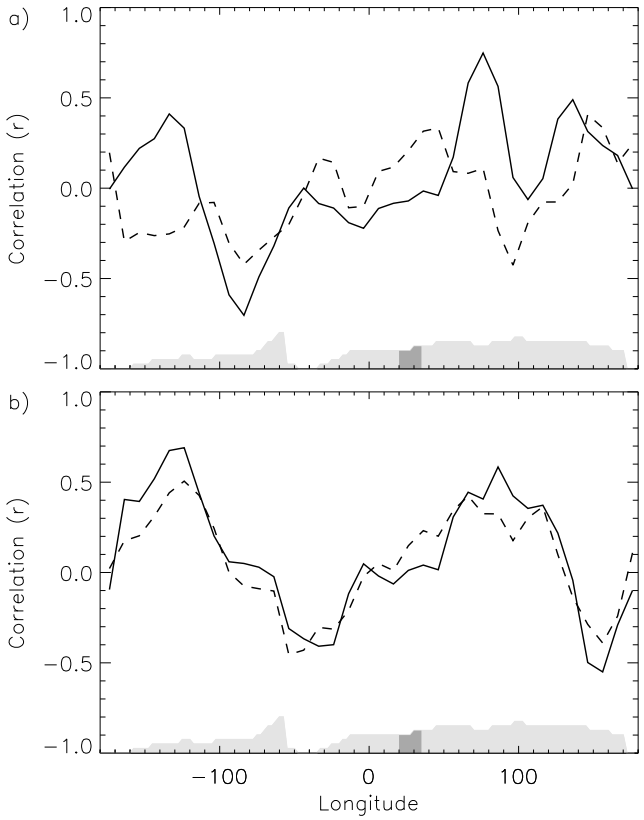

Figure 8. (a) Correlation coefficients between sea ice extent for each point around the Antarctic continent and MSA snow concentration (solid line) and MSA deposition flux (dashed line) at a single location for the capped run and (b) difference between the uncapped and capped runs. Antarctica is shown as a shaded region along the x-axis for reference. Sea ice extent was averaged over 15° sectors, and MSA snow concentration/deposition flux was averaged over the region 20°E–35°E, between the coast and 74°S (dark shading).

concentration measurements exhibit an increasing gradient from the coast toward the interior of the East Antarctic Plateau, due to a decreasing snow accumulation gradient inland from the coast in the same region (Figure 2). This increasing gradient is captured by the model. The lower precipitation rate causes a shift toward an increased fraction of MSA loss via dry deposition in inland Antarctica. Post-depositional processes such as surface snow redistribution and intra-seasonal diffusion of MSA peaks within firn [*Weller et al.*, 2004; *Wagnon et al.*, 1999] are not incorporated into the model. The observations in Figure 7 include both surface snow and ice core concentrations and may be influenced by post-depositional processes. In general these processes need to be understood well enough to interpret longer ice core records, but they are not relevant for the idealized analysis in our study.

4. Results

4.1. Relationship Between Sea Ice Extent and MSA Snow Concentrations and MSA Deposition Flux

[37] To mimic the analysis that is frequently done with MSA concentrations recorded in ice cores to find patterns of correlation with nearby sea ice extent, we create two MSA-sea ice metrics – correlation of each of the time series of MSA snow concentration and MSA deposition flux at one location in the model with sea ice extent around the continent. We correlate each MSA time series with the time series of the latitude of sea ice extent averaged in 15° longitudinal sectors around the continent. If the sea ice exerts sufficient influence on DMS emissions, we expect negative correlation coefficients in both MSA-sea ice metrics for nearby sea ice extent in the Simó and Dachs capped run. We isolate the effect of DMS emissions from the sea ice itself and also compute the MSA-sea ice metrics for the difference between the Simó and Dachs uncapped and capped scenarios, for which we expect positive correlation coefficients for nearby sea ice extent given that this isolates DMS emissions from the sea ice.

[38] Figure 8a presents the MSA-sea ice metrics for a coastal area between 20°E and 35°E as an example of a location in the model that demonstrates relatively strong correlation coefficients compared to other locations. In the Simó and Dachs capped run, we find correlation coefficients for MSA snow concentration with sea ice in 15° sectors in the range of r = −0.75 to +0.75, and for MSA deposition flux with sea ice in the same sectors in the range of r = −0.4 to +0.4, as shown in Figure 8a. The magnitude of the modeled correlation coefficients are similar to the observations [e.g., *Curran et al.*, 2003; *Abram et al.*, 2007]. We expect the strongest negative correlation coefficients between the model MSA deposition flux/snow concentration and sea ice extent in adjacent sectors and/or upwind given the prevailing Southern Ocean westerlies and southeastward-moving storm tracks [e.g., *Yuan et al.*, 2009]. However, we find no consistency in the pattern or sign of correlation coefficients for this location in the Simó and Dachs capped run. The same MSA-sea ice metrics computed for the Simó and Dachs uncapped run (not shown) are similar in sign and magnitude, yet the Simó and Dachs uncapped runs by design eliminate any mechanistic relationship between sea ice extent and MSA in Antarctica.

[39] Figure 8b shows same MSA-sea ice metrics for the difference between the Simó and Dachs uncapped and capped runs. The correlation coefficients are of magnitudes similar to those found for the Simó and Dachs capped run, yet again the pattern is inconsistent with our expectations. The correlation coefficients are near zero between MSA deposition flux/snow concentration and the adjacent sea ice extent. Positive correlation coefficients occur too far to the west of the selected location to indicate significant influence of sea ice on MSA.

[40] Examination of the same MSA-sea ice metrics from other locations on Antarctica yield similar magnitudes of correlation coefficients between MSA deposition flux/snow concentration and sea ice extent, but no physically credible explanations. In the remainder of the paper, we seek to understand why no sea ice-MSA relationship is apparent in the model, and focus on the relationship between sea ice extent and DMS emissions. We discuss fundamental differences between the global and high-latitude sulfur budgets that lead to longer DMS and MSA lifetimes, determine the zonal deposition pattern of sulfur species (SO_2, $nssSO_4^{2-}$, MSA) originating from the sea ice (from the difference between the uncapped and capped runs), and estimate the

Table 3. Total DMS Emissions for South of 60°S and Total MSA Deposition to Antarctica

Simulation	DMS Data Set[a]	Emissions Parameterization[a]	DMS Emissions[b] (Gg S)	Antarctica MSA Deposition[b] (Gg S)
Simó and Dachs capped	SD2002	N2000	361 ± 26	15.3 ± 1.5
Simó and Dachs uncapped	SD2002	N2000	409 ± 29	16.0 ± 1.6
Simó and Dachs enhanced	SD2002	N2000	646 ± 44	19.1 ± 1.7
Sensitivity simulations				
Huebert2010 capped	SD2002	H2010	281 ± 20[d]	9.8 ± 1.0[d]
Huebert2010 uncapped	SD2002	H2010	328 ± 23[d]	10.4 ± 1.0[d]
BrO capped	SD2002	N2000	366 ± 26[d]	19.6 ± 2.3
BrO uncapped	SD2002	N2000	417 ± 29[d]	21.0 ± 2.2
GEOS-5 capped	SD2002	N2000	333 ± 24[d]	4.9 ± 0.5[d]
GEOS-5 uncapped	SD2002	N2000	396 ± 28[d]	5.3 ± 0.5[d]
Kettle1999 capped	K1999	N2000	1026 ± 38	24.0 ± 2.8
Kettle1999 uncapped	K1999	N2000	1351 ± 72	29.5 ± 3.3
Lana2011 capped	L2011	N2000	769 ± 54[c]	—[d]
Lana2011 uncapped	L2011	N2000	976 ± 68[c]	—[d]

[a]Abbreviations: SD2002, *Simó and Dachs* [2002]; N2000, *Nightingale et al.* [2000]; H2010, *Huebert et al.* [2010]; K1999, *Kettle et al.* [1999]; L2011, *Lana et al.* [2011].
[b]Emissions fluxes and deposition fluxes are time and spatially integrated over the 6 month period October–March.
[c]Uncertainties estimated at same percentage as capped run.
[d]Lana2011 simulations were conducted to estimate DMS emissions in GEOS-Chem only.

fraction of Antarctic MSA that originates in the Southern Ocean south of 60°S. We also estimate the relative contribution of the variability in sea ice extent and wind speed to variability in DMS emissions.

4.2. Regional Sulfur Budget

[41] We consider the regional sulfur budget for October–March to examine how the southern high-latitudes deviate from global averages. Table 3 shows the October–March DMS emissions south of 60°S and MSA deposition on the Antarctic continent for all simulations. We find that DMS emissions in the region south of 60°S increase by 13% and 79% in the Simó and Dachs uncapped and enhanced runs over the capped run, respectively. MSA deposition to Antarctica, however, increases by only 4% and 19% respectively. DMS emissions from sea ice have a large effect on regional sulfur emissions; however, the MSA deposition to the Antarctic continent does not increase proportionally.

[42] In the capped simulation, the October-March DMS lifetime south of 60°S (4.0 days) is about three times greater than the global mean (1.3 days) due to lower oxidant concentrations in the high latitudes. The October–March lifetime of MSA south of 60°S is 9.2 days compared to 6.7 days for the global mean. The lower scavenging efficiency at colder temperatures and lower precipitation rates on Antarctica lead to the longer MSA lifetime. The lengthening of both the MSA and DMS lifetimes in the high southern latitudes implies an increased potential for long range transport of chemical species in the region and smoothing of any local DMS signal in MSA deposition patterns. The lengthening of DMS and MSA lifetimes at high latitudes is not present in the BrO sensitivity simulations (see section 4.6), suggesting that this is dependent on our understanding of the high-latitude oxidation mechanism of DMS. Lifetimes for the Simó and Dachs uncapped and enhanced runs are not significantly different in the southern high latitudes from those of the Simó and Dachs capped run. Regional lifetimes in the GEOS-5 sensitivity simulations are different from the GEOS-4 simulations and are discussed in more detail below, but lead to the same conclusions.

4.3. Distribution of MSA Deposition From DMS Emissions in Sea Ice

[43] Figure 9 shows the zonal distributions of DMS emissions from the sea ice and sulfur deposition (sum of SO_2, $nssSO_4^{2-}$, and MSA) calculated from the difference between the Simó and Dachs uncapped and capped runs. Net transport of sulfur species from the sea ice zone is northward. The DMS emissions distribution peaks at 66°S, but sulfur deposition peaks at 60°S, with roughly half of the deposition to the north of 60°S. Of the sulfur emitted from the sea ice (i.e., in the difference between the Simó and Dachs uncapped and capped simulations), only 7.7% is deposited on the Antarctic continent. This ranges from as low as 4.1% for the GEOS-5 sensitivity simulations to as high as 9.6% in the Kettle1999 sensitivity simulations.

[44] Figure 10 shows the mean October–March MSA snow concentrations resulting from DMS emissions only

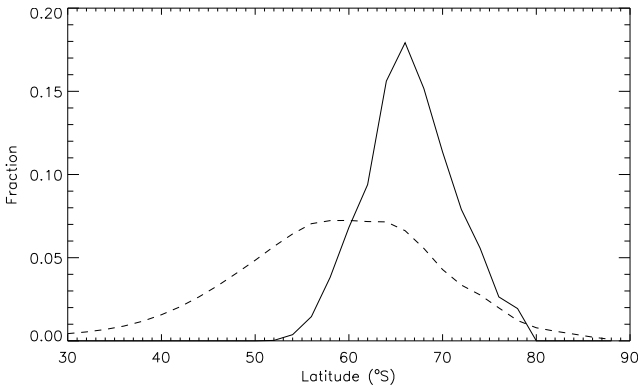

Figure 9. The fraction of DMS emitted at each latitude relative to the total DMS emissions for October through March from the difference between the Simó and Dachs uncapped and capped runs (solid line). The fraction of sulfur deposition at each latitude relative to the total sulfur deposition (dashed line). Sulfur deposition includes the sum of SO_2, $nssSO_4^{2-}$, and MSA, and is conserved with respect to DMS emissions in the difference between the uncapped and capped runs.

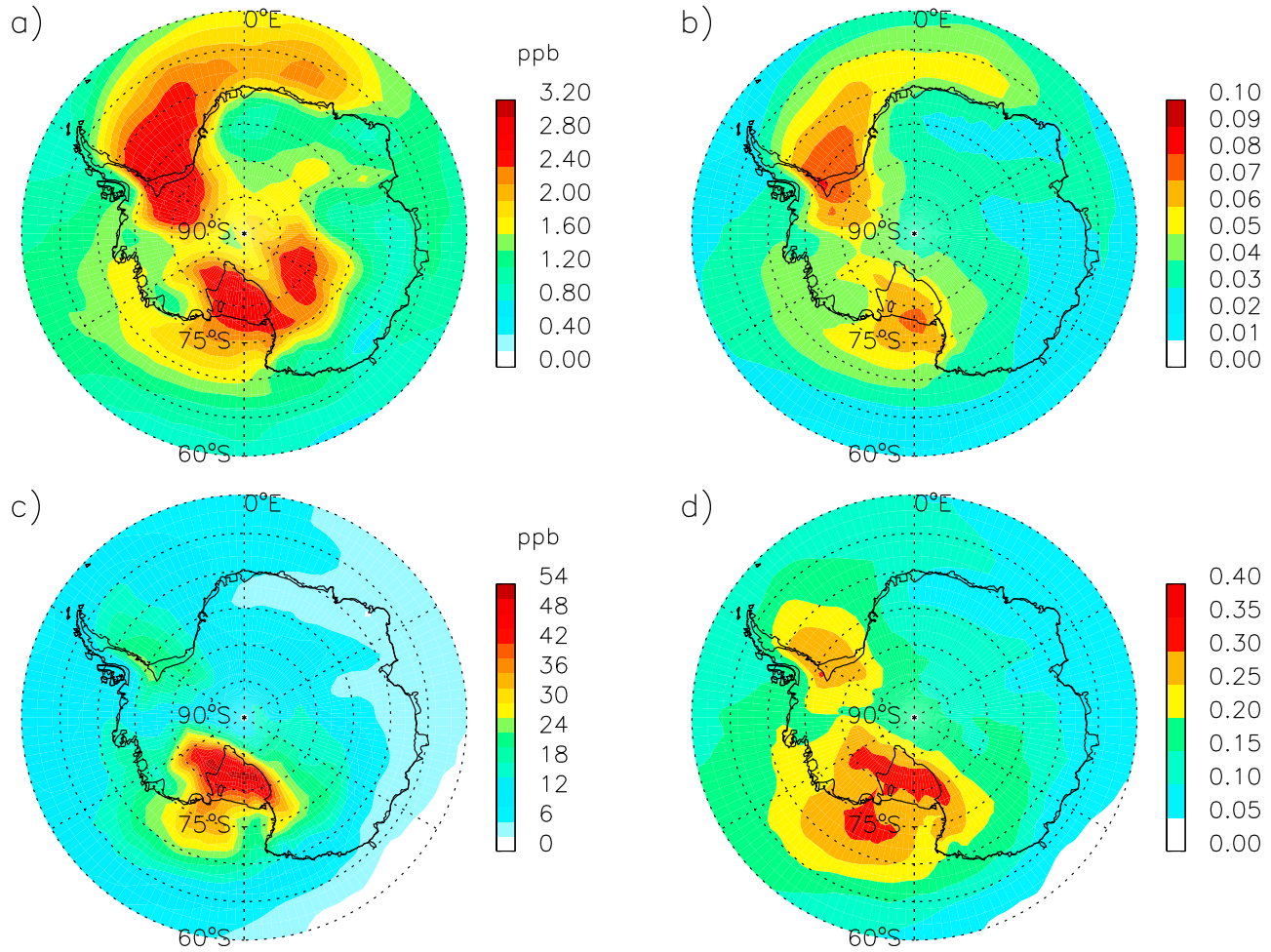

Figure 10. (a) MSA snow concentration (ppb) from DMS emissions in the sea ice zone (difference between the Simó and Dachs uncapped and capped runs), and (b) fraction of MSA deposition originating from the sea ice in the Simó and Dachs uncapped run. (c and d) The same as Figures 10a and 10b for the Kettle1999 uncapped and capped simulations.

from the sea ice (uncapped minus capped) and the fraction this contributes to the uncapped simulation ([uncapped – capped]/uncapped) in both the Simó and Dachs and the Kettle1999 simulations. In the Simó and Dachs uncapped run, DMS emissions from the sea ice zone are small, so only a small fraction of the MSA deposited on Antarctica comes from DMS emitted in the sea ice at any given continental location (Figures 10a and 10b). The hot-spots of DMS concentration in the Kettle99 uncapped run (See Figure 1b) translate to a greater contribution from sea ice to MSA deposition in Antarctica, especially in the Ross Sea sector (Figures 10c and 10d). The relative importance of MSA derived from DMS in sea ice to total MSA snow concentrations is highly dependent upon seawater DMS concentrations within the sea ice zone, but in all simulations represents <25% of total MSA deposition throughout most of Antarctica.

[45] Interannual variability in circumpolar sea ice extent in the Southern Ocean has been shown by *Zwally et al.* [2002] to be on the order of 8% (1%) of the summer (winter) mean areal extent, with maximum variability by sector of 25% in the summer extent in the Ross Sea (160°E–60°W) and 11% in winter in the Bellingshausen/Amundsen Seas (130°–60°W). Absent a mechanism whereby the interannual signal of sea ice on DMS emissions is amplified, we would expect interannual variation in DMS emissions associated with the variation in sea ice to be commensurate with interannual variation in sea ice extent. Given the relatively small fractional contribution of sea ice to MSA deposition at most locations on the continent (Figures 10b and 10d) and the relatively small interannual variability in sea ice extent compared to the mean ice extent, it is not surprising that we are unable to associate MSA deposition variability with DMS emissions variability due to changes in sea ice at most locations on the Antarctic continent.

4.4. Estimation of DMS Emissions South of 60°S Necessary to Dominate Antarctic MSA Deposition

[46] A solid quantitative understanding of the DMS emissions, not just surface DMS concentrations, from within the sea ice zone is imperative. The magnitude of DMS emissions in the sea ice zone (i.e., south of 60°S) determines whether deposition of MSA and other sulfur species to the Antarctic continent is dominated by DMS emissions influenced by sea ice. Since the duration and timing of elevated

sea surface DMS concentrations in the wake of the seasonal retreat of sea ice are not established and we do not attempt to model them in our scenarios here, we use the region south of 60°S as an estimate of the maximum areal extent of DMS emissions influenced by the seasonal cycle of sea ice. We then determine the contribution of DMS emissions from this area to Antarctic MSA deposition. The fractional contribution of DMS emissions from south of 60°S to MSA deposition in Antarctica is larger than that shown in Figures 10b and 10d because the area south of 60°S is larger than the area covered by sea ice.

[47] In the Simó and Dachs uncapped run, the October-March average of DMS emissions in the region south of 60°S is 100 μg S m^{-2} d^{-1} and represents 26–30% (36–42%) of the total MSA deposition at the coast (inland). Coastal areas are defined as coastal grid boxes for Antarctica plus one grid box to the north and south (±2° latitude) to estimate marine influence, and inland areas are defined as grid boxes poleward of coastal areas. To be the dominant source (i.e., >50%) of MSA deposition at the coast (inland), DMS emissions south of 60°S would need to increase by a factor of 1.6 (1.2). For the region south of 60°S to supply 80% of MSA at the coast (inland), DMS emissions would need to increase by a factor of 9–10 (6). *Curran and Jones* [2000] calculated a mean spring through summer surface DMS emissions flux of 300 μg S m^{-2} d^{-1} based on observed surface DMS concentrations in the Australian sector of the Southern Ocean (65°E to 162°E) and the *Liss and Merlivat* [1986] ocean-air gas transfer parameterization. The reported fluxes range from 54 μg S m^{-2} d^{-1} in the spring to the north of the sea ice to 1570 μg S m^{-2} d^{-1} in the summer in the seasonal sea ice zone. Thus, DMS emissions ~1000 μg S m^{-2} d^{-1} are clearly possible but may be episodic. MSA deposition in the Kettle1999 simulations is already dominated by DMS emissions from south of 60°S, representing 54–62% (84–95%) of coastal (inland) MSA. Mean October–March DMS emissions south of 60°S in the Kettle1999 uncapped run are 320 μg S m^{-2} d^{-1}.

[48] The new DMS data set constructed by *Lana et al.* [2011] from updated measurements in the Global Surface Seawater Database reduces the magnitude and extent of seasonal hot-spots in DMS concentrations around Antarctica in the austral summer (Figure 1e) compared to the Kettle1999 data set (Figure 1c), which implies DMS concentrations and hence emissions in our Kettle1999 simulations are overestimated. The emissions estimates based on work by *Lana et al.* [2011] are bracketed by the DMS emissions estimates from Simó and Dachs and Kettle1999 data sets both globally (section 3.1) and regionally south of 60°S (Table 3). *Lana et al.* [2011] do not address the question of DMS emissions estimates from within sea ice in their paper, and so the seasonal cycle and magnitude of DMS emissions from sea ice itself remains an open question.

4.5. Controls on DMS Emissions Variability: Relative Influence of Sea Ice Extent and Wind Speeds

[49] Here we seek to understand the model controls on DMS emissions in the Southern Ocean and just how strongly the DMS emissions are modulated by the variability in sea ice and the variability in wind. We first examine the relationship between DMS emissions south of 60°S and the latitude of mean October–March sea ice extent in the Simó and Dachs and Kettle1999 capped runs (Figure 11), and for the difference in emissions between the respective uncapped and capped runs (Figure 12). The Southern Ocean between 60°S and the Antarctic coast is divided into 15° longitudinal sectors and a time series of sea ice extent and DMS emissions is computed from the October–March mean in each sector. While recognizing that sea ice extent and DMS emissions in some sectors may have stronger correlations than in other sectors, we combine the time series from all sectors into a single scatter plot and compute a single correlation coefficient to represent general circumpolar relationships. We do the same to examine the relationship between DMS emissions and mean wind speed in each sector.

[50] We expect the strongest relationship between sea ice extent and DMS emissions in our runs that have the largest gradient in DMS surface concentration across the ice edge. The strongest gradient exists in the Kettle1999 capped simulation (see Figure 1c), and thus we see the strongest correlation (r^2 = 0.30) between DMS emissions and sea ice extent in the Kettle1999 capped run (Figure 11c). The much weaker gradient in the Simó and Dachs data set results in a much smaller correlation (r^2 = 0.11) between sea ice extent and DMS emissions in the Simó and Dachs capped run (Figure 11a). The sea ice extent-DMS emissions relationship is weak in the Simó and Dachs capped run, and so the winds become a more important factor (r^2 = 0.46; Figure 11b).

[51] The relationship between sea ice extent and DMS emissions for the difference between the Simó and Dachs uncapped and capped runs, which isolates DMS emissions from sea ice only, is shown in Figure 12a. As expected for DMS emissions restricted to the sea ice, there is a positive relationship between sea ice extent and DMS emissions. Surprisingly, at most only 60% of the variability in DMS emissions can be explained by variations in sea ice extent itself. Emissions isolated from the sea ice in the Kettle1999 data set yield a weaker positive relationship between sea ice extent and DMS emissions (r^2 = 0.34, Figure 12c) than the emissions isolated from the sea ice for the Simó and Dachs data set. In neither case does wind speed explain much of the variability of DMS emissions (r^2 < 0.07) for emissions isolated from the sea ice (Figures 12b and 12d).

[52] We expected a fairly strong relationship between sea ice extent and DMS emissions in our capped scenarios (both Simó and Dachs and Kettle1999) given the prescribed gradient in DMS concentrations across the sea ice edge. Seasonal attribution of DMS emissions variability, however, is strongly dependent on the characteristics of the underlying surface seawater DMS concentration data set. The weak correlation between DMS emissions and sea ice extent in the Simó and Dachs capped run is a consequence of the interplay between the characteristics of DMS concentrations (magnitude, seasonal cycle, and meridional gradients), the seasonal cycle of ice extent, and the relative contribution of wind speed. Wind speed plays a dominant role in the Simó and Dachs capped simulation because of the combination of increasing wind speeds and increasing DMS concentrations equatorward. The stronger role of sea ice variability and reduced role of wind in the Kettle1999 sensitivity simulations can be ascribed to a combination of a stronger gradient of DMS concentrations across the ice edge in the Kettle1999 capped simulation, the increasing DMS concentrations

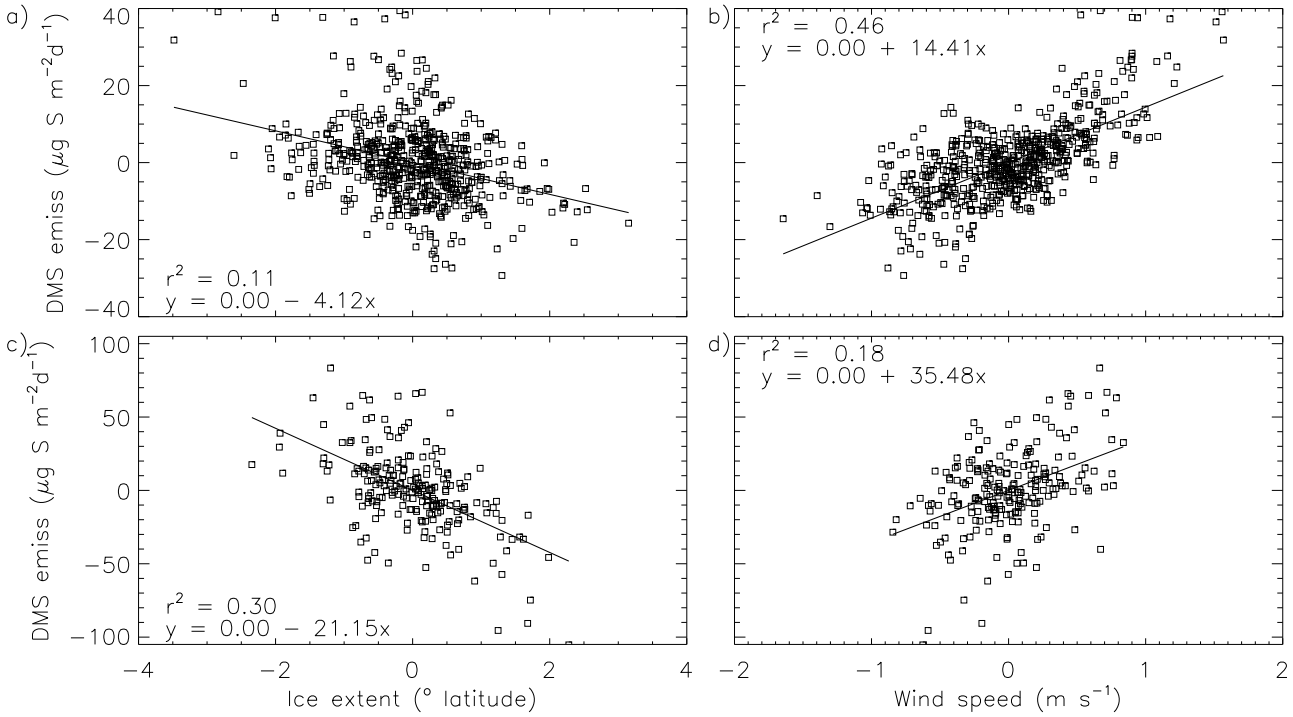

Figure 11. Correlation of (a) DMS emissions anomalies (μg S m^{-2} d^{-1}) versus sea ice extent anomalies (° latitude) ($r^2 = 0.11$), and (b) DMS emissions anomalies versus wind speed anomalies (m s^{-1}) ($r^2 = 0.46$) for Simó and Dachs capped run and (c) ($r^2 = 0.30$) and (d) ($r^2 = 0.18$) for the Kettle1999 capped run. Time series of seasonal October–March means are computed over 15° sectors south of 60°S for each field, and all sectors are combined to compute the correlation.

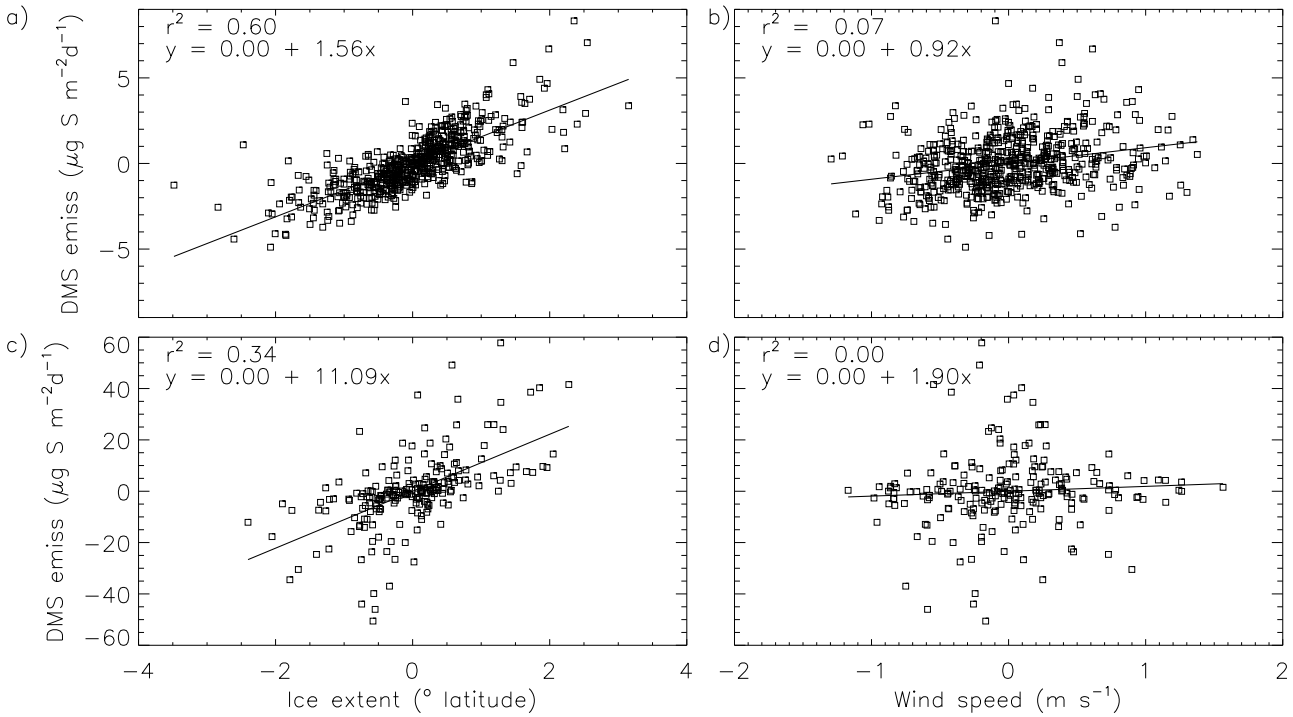

Figure 12. Same as Figure 11 for difference between Simó and Dachs uncapped and capped runs (a) ($r^2 = 0.60$) and (b) ($r^2 = 0.07$), and difference between Kettle1999 uncapped and capped runs (c) ($r^2 = 0.34$) and (d) ($r^2 < 0.01$).

poleward, and the influence of a stronger seasonal cycle of DMS surface concentrations in the Kettle1999 data set.

[53] When DMS emissions exclusively from the sea ice area are considered, (i.e., the difference between the uncapped and capped scenarios), we find that the sea ice variability explains only a fraction of the variability in DMS emissions (34–60%), for both the Simó and Dachs and Kettle1999 simulations. This is in spite of the fact that ice expands northward into regions associated with generally higher mean wind speeds. For sea ice to dominate the variability in DMS emissions in the sea ice zone, the effect of stronger winds north of the sea ice must be compensated by strong DMS emissions associated with the sea ice itself. A better understanding of the peculiarities of DMS emissions from within the sea ice is important for understanding whether DMS emissions in the Southern Ocean are dominated by variability in sea ice extent.

4.6. Sensitivity to BrO Oxidation Mechanism

[54] The BrO sensitivity simulation results in a 55% increase in the global annual MSA production rate. The increase in MSA production leads to a commensurate increase in October-March MSA deposition in Antarctica of 49%. However, the addition of BrO chemistry does not change the fraction of sulfur deposition to Antarctica that originates from sea ice (~7%).

[55] The addition of the BrO oxidation pathway induces more rapid DMS oxidation in the high latitude boundary layer which leads to shorter DMS lifetimes. The lifetime of DMS in the high latitudes decreases to 0.9–1.1 days for October–March, and unlike the Simó and Dachs simulations, has no meridional gradient approaching the poles. Increased production of MSA in the boundary layer results in more efficient deposition and leads to shorter MSA lifetimes south of 60°S. The lifetime of MSA south of 60°S decreases to 5.6 days for October–March, compared to 8.9 days in the Simó and Dachs capped simulation. The yield of MSA from DMS oxidation increases to 34% in the BrO simulation from 17% in the Simó and Dachs simulations for the high latitudes south of 60°S.

[56] The net transport of sulfur species originating from DMS emissions from the sea ice remains northward though the distribution is narrower than the Simó and Dachs simulations (see Figure 9); 50% is deposited to the north of 62°S. The sensitivity of MSA deposition to DMS emissions from the sea ice is nearly doubled in coastal regions compared to the Simó and Dachs simulations (see Figure 10b), and accounts for up to 20% of MSA deposition in the Ross, Amundsen-Bellingshausen, and Weddell seas regions along the coast (not shown). The sensitivity in the interior of the East Antarctic Plateau is approximately the same. The local (i.e., south of 60°S) source of MSA to the coastal (inland) areas of Antarctica increases to 46–48% (52–57%) compared to 26–30% (36–42%) in the Simó and Dachs simulations (see section 4.4).

[57] The shortening of the modeled DMS and MSA lifetimes under the BrO sensitivity simulation improves the probability of retaining an ice core signal of local DMS emissions from sea ice. The three year sensitivity simulation however is too short to estimate correlations between MSA and sea ice extent/DMS emissions. Since DMS from south of 60°S in the BrO sensitivity simulations still does not dominate MSA deposition in Antarctica and there is still relatively small interannual variability in sea ice extent during this time period, we would not expect correlations between MSA and sea ice extent to be significantly improved. It does, however, warrant further study, with a more careful implementation of the BrO oxidation scheme.

4.7. Sensitivity to GEOS-5 Meteorology

[58] Here we investigate the sensitivity of our results to the underlying meteorological fields driving the model. The boundary layer is not well resolved in GEOS-4 meteorological reanalysis which might lead to an overestimation of the exchange between the boundary layer and the free troposphere and hence an overestimation of both DMS and MSA lifetimes. A GEOS-5 sensitivity study (Table 1) has been performed with the GEOS-5 meteorological fields, which have a higher boundary layer resolution of 13 layers in the lowest 2 km of the atmosphere, compared to 4.5 layers in GEOS-4.

[59] These sensitivity simulations result in a shorter global October–March lifetime of DMS and MSA by 8% and 27% respectively compared to the capped simulation, which is significant with respect to the range of variability within the capped run (1.5% and 5% respectively). Since oxidant fields are unchanged and DMS is unaffected by changes in precipitation in GEOS-5, the main difference in the DMS lifetime between using the GEOS-4 and GEOS-5 reanalysis is related to the increased boundary layer resolution. Though the global DMS lifetime is shorter (by 8%) because of globally reduced vertical transport to the free troposphere in the GEOS-5 simulations, the DMS lifetimes calculated for the region south of 60°S and the Antarctic continent in the GEOS-5 capped sensitivity run fall consistently within the range of lifetimes found in the capped run.

[60] Changes in precipitation play a role in the changes in regional MSA lifetimes in the GEOS-5 sensitivity runs. MSA lifetimes are substantially shorter in the global mean (27%), shorter for south of 60°S (11%), and much longer (by more than a factor of 2) over Antarctica, all outside the range of lifetimes found for the capped run. The precipitation between 30°S and 60°S increases by 25–100% in the GEOS-5 reanalysis relative to GEOS-4, a correction of the low bias noted by *Bloom et al.* [2005]. This leads to shorter lifetimes and lower burdens in air masses entering the high latitudes and therefore less transport of sulfur species toward the pole. Indeed, as discussed above, in the GEOS-5 sensitivity simulations only 4.1% of sulfur emitted from the sea ice is deposited in Antarctica, compared to 7.7% for the GEOS-4 Simó and Dachs simulations. The substantial increase in MSA lifetime over Antarctica is caused by the decrease in precipitation over the Antarctic continent which causes an increase in the fraction of MSA loss via dry deposition (31%, compared to 18% using GEOS-4). The area dominated by dry deposition in GEOS-4 is confined to the East Antarctic Plateau, with a gentle gradient toward more wet deposition at the coasts. In the GEOS-5 simulation, the area dominated by dry deposition expands greatly, leaving only coastal areas and the Ronne, Filchner and Ross ice shelves dominated by wet deposition. The transition between regions dominated by dry and wet deposition occurs over a much shorter spatial scale in the GEOS-5 simulation. Despite the impact of the meteorological fields on the spatial distribution of MSA wet

and dry deposition, the GEOS-5 sensitivity simulations show that DMS emissions from south of 60°S account for 35–40% (50–61%) of coastal (inland) MSA deposition to Antarctica, which is similar to the results for the Simó and Dachs runs with GEOS-4.

5. Conclusions

[61] We have run a series of global chemical transport model (GEOS-Chem) simulations in an effort to better understand the spatial patterns of MSA deposition and snow concentrations in Antarctica and its relationship to sea ice. Simulations span the period 1985 through 2004, forced with assimilated GEOS meteorological data and observed sea ice extent. We varied the sea surface DMS concentrations associated with sea ice over the austral summer from October through March to understand the influence of DMS emissions from the sea ice zone on the oxidation of DMS to MSA and the transport and deposition of MSA to the Antarctic continent. Our model scenarios by construction implement a relationship between sea ice extent and DMS sea surface concentrations. We estimated correlation coefficients of MSA concentrations in snow with sea ice extent within the model. The model can reproduce the magnitude of correlation coefficients but not the spatial relationship of correlation coefficients reported in ice core studies.

[62] We find that the net transport of DMS emissions from the sea ice zone is northward and only a small fraction (4–9.6%) of sulfur emissions from the sea ice zone is deposited in Antarctica. The fraction of MSA deposition that originates from DMS in the sea ice zone (i.e., from south of 60°S) ranges from 26–95%, depending on the simulation and region of Antarctica. This result is strongly dependent on the absolute magnitude of emissions in the sea ice zone. In order for Antarctic MSA deposition to be dominated (i.e., >50%) by DMS emissions within the sea ice zone, sustained DMS emissions throughout austral spring and summer would need to be on the order of 120–160 μg S m^{-2} d^{-1}, which falls within the wide range of observations [e.g., *Curran and Jones*, 2000]. More complete information about the magnitude of high-latitude seawater DMS concentrations and the influence of sea ice on DMS emissions is crucial.

[63] Lifetimes of both DMS and MSA are highly sensitive to the presence of halogen oxidants. Without oxidation of DMS by BrO, high latitude lifetimes of DMS and MSA are longer than in the global means and local and regional signals of DMS emissions would be expected to be diluted by transport and mixing. Inclusion of a BrO oxidation mechanism demonstrates a strong relative importance of this pathway at high latitudes and improves the potential for retaining a local signal of DMS emissions in MSA deposition in Antarctica.

[64] In order for MSA recorded in ice cores to be related to sea ice extent, not only must DMS emissions from the sea ice zone be the dominant source region of MSA to Antarctica but sufficient variability of DMS emissions must be attributed to sea ice variability (as opposed to variability related to other factors such as wind speeds). We find that the variability in sea ice extent explains only 11–30% of the variability of DMS emissions south of 60°S, and only 34–60% of the variability of DMS emissions when considering only DMS emissions from the sea ice itself. This is consistent with the findings of *Preunkert et al.* [2007], who reported a poor correlation of DMS seawater concentrations with sea ice extent, and might be expected given the small interannual variability in sea ice extent compared to the area over which DMS emissions in the Southern Ocean are derived. Wind speeds also play a role in DMS emissions variability, but the relative influence of sea ice extent compared to wind speed on DMS emissions is dependent on the seasonal cycle, magnitude, and meridional gradients of the seawater DMS concentrations. In addition to a need for improved information about seawater DMS concentrations in the sea ice zone, information on the sea-to-air transfer of DMS from sea ice and its dependence on physical factors such as wind speed and SST are crucial for evaluation of the importance of sea ice on Southern Ocean DMS emissions and the resulting MSA deposition to Antarctica. Our analysis has focused on present-day conditions and sea ice extents on interannual timescales. Interpretation of MSA deposition in ice core records on glacial-interglacial timescales, for which variability in sea ice extent is much larger, remains an open question.

[65] **Acknowledgments.** This project was supported through NSF grant ANT-0739127. The authors would like to thank A. Lana and R. Simó for providing the gridded Simó and Dachs DMS data set, and N. Bertler for providing the data set of Antarctic snow and ice core MSA measurements. Measurements performed at Amsterdam Island were supported by the French Polar Institute (IPEV) within the AEROTRACE program. The authors would also like to thank S. Elliott and two anonymous reviewers for comments and suggestions that strengthened and improved the manuscript.

References

Abram, N. J., R. Mulvaney, E. W. Wolff, and M. Mudelsee (2007), Ice core records as sea ice proxies: An evaluation from the Weddell Sea region of Antarctica, *J. Geophys. Res.*, *112*, D15101, doi:10.1029/2006JD008139.

Abram, N. J., E. R. Thomas, J. R. McConnell, R. Mulvaney, T. J. Bracegirdle, L. C. Sime, and A. J. Aristarain (2010), Ice core evidence for a 20th century decline of sea ice in the Bellingshausen Sea, Antarctica, *J. Geophys. Res.*, *115*, D23101, doi:10.1029/2010JD014644.

Alvarez-Aviles, L., W. R. Simpson, T. A. Douglas, M. Sturm, D. Perovich, and F. Domine (2008), Frost flower chemical composition during growth and its implications for aerosol production and bromine activation, *J. Geophys. Res.*, *113*, D21304, doi:10.1029/2008JD010277.

Ayers, G. P., S. T. Bentley, J. P. Ivey, and B. W. Forgan (1995), Dimethylsulfide in marine air at Cape Grim, 41°S, *J. Geophys. Res.*, *100*(D10), 21,013–21,021.

Barnes, I., J. Hjorth, and N. Mihalopoulos (2006), Dimethyl sulfide and dimethyl sulfoxide and their oxidation in the atmosphere, *Chem. Rev.*, *106*(3), 940–975.

Becagli, S., et al. (2009), Methanesulphonic acid (MSA) stratigraphy from a Talos Dome ice core as a tool in depicting sea ice changes and southern atmospheric circulation over the previous 140 years, *Atmos. Environ.*, *43*(5), 1051–1058.

Berglen, T. F., T. K. Berntsen, I. S. A. Isaksen, and J. K. Sundet (2004), A global model of the coupled sulfur/oxidant chemistry in the troposphere: The sulfur cycle, *J. Geophys. Res.*, *109*, D19310, doi:10.1029/2003JD003948.

Bertler, N., et al. (2005), Snow chemistry across Antarctica, *Ann. Glaciol.*, *41*, 167–179.

Bey, I., D. J. Jacob, R. M. Yantosca, J. A. Logan, B. D. Field, A. M. Fiore, Q. B. Li, H. G. Y. Liu, L. J. Mickley, and M. G. Schultz (2001), Global modeling of tropospheric chemistry with assimilated meteorology: Model description and evaluation, *J. Geophys. Res.*, *106*(D19), 23,073–23,095.

Bloom, S., et al. (2005), Documentation and validation of the Goddard Earth Observing System (GEOS) data assimilation system - version 4, *Tech. Rep. 104606*, NASA Goddard Space Flight Cent., Greenbelt, Md.

Boucher, O., M. Pham, and C. Venkataraman (2002), Simulation of the atmospheric sulfur cycle in the Laboratoire de Meteorologie Dynamique General Circulation Model. Model description, model evaluation, and global and European budgets, *Note 23*, IPSL, Paris.

Boucher, O., et al. (2003), DMS atmospheric concentrations and sulphate aerosol indirect radiative forcing: A sensitivity study to the DMS source representation and oxidation, *Atmos. Chem. Phys.*, *3*, 49–65.

Breider, T. J., M. P. Chipperfield, N. A. D. Richards, K. S. Carslaw, G. W. Mann, and D. V. Spracklen (2010), Impact of BrO on dimethylsulfide in

the remote marine boundary layer, *Geophys. Res. Lett.*, *37*, L02807, doi:10.1029/2009GL040868.
Cameron-Smith, P., S. Elliott, M. Maltrud, D. Erickson, and O. Wingenter (2011), Changes in dimethyl sulfide oceanic distribution due to climate change, *Geophys. Res. Lett.*, *38*, L07704, doi:10.1029/2011GL047069.
Castebrunet, H., C. Genthon, and P. Martinerie (2006), Sulfur cycle at Last Glacial Maximum: Model results versus Antarctic ice core data, *Geophys. Res. Lett.*, *33*, L22711, doi:10.1029/2006GL027681.
Chatfield, R. B., and P. J. Crutzen (1990), Are there interactions of iodine and sulfur species in marine air photochemistry, *J. Geophys. Res.*, *95*(D13), 22,319–22,341.
Chin, M., D. J. Jacob, G. M. Gardner, M. S. Foreman-Fowler, P. A. Spiro, and D. L. Savoie (1996), A global three-dimensional model of tropospheric sulfate, *J. Geophys. Res.*, *101*(D13), 18,667–18,690.
Chin, M., R. B. Rood, S. J. Lin, J. F. Muller, and A. M. Thompson (2000), Atmospheric sulfur cycle simulated in the global model GOCART: Model description and global properties, *J. Geophys. Res.*, *105*(D20), 24,671–24,687.
Corbett, J. J., P. S. Fischbeck, and S. N. Pandis (1999), Global nitrogen and sulfur inventories for oceangoing ships, *J. Geophys. Res.*, *104*(D3), 3457–3470.
Cosme, E., C. Genthon, P. Martinerie, O. Boucher, and M. Pham (2002), The sulfur cycle at high-southern latitudes in the LMD-ZT General Circulation Model, *J. Geophys. Res.*, *107*(D23), 4690, doi: 10.1029/2002JD002149.
Cosme, E., F. Hourdin, C. Genthon, and P. Martinerie (2005), Origin of dimethylsulfide, non-sea-salt sulfate, and methanesulfonic acid in Eastern Antarctica, *J. Geophys. Res.*, *110*, D03302, doi:10.1029/2004JD004881.
Curran, M. A. J., and G. B. Jones (2000), Dimethyl sulfide in the Southern Ocean: Seasonality and flux, *J. Geophys. Res.*, *105*(D16), 20,451–20,459.
Curran, M. A. J., T. D. van Ommen, V. I. Morgan, K. L. Phillips, and A. S. Palmer (2003), Ice core evidence for Antarctic sea ice decline since the 1950s, *Science*, *302*(5648), 1203–1206.
de Boyer-Montegut, C., G. Madec, A. S. Fischer, A. Lazar, and D. Iudicone (2004), Mixed layer depth over the global ocean: An examination of profile data and a profile-based climatology, *J. Geophys. Res.*, *109*, C12003, doi:10.1029/2004JC002378.
Delille, B., B. Jourdain, A. V. Borges, J. L. Tison, and D. Delille (2007), Biogas (CO_2, O_2, dimethylsulfide) dynamics in spring Antarctic fast ice, *Limnol. Oceanogr.*, *52*(4), 1367–1379.
Elliott, S. (2009), Dependence of DMS global sea-air flux distribution on transfer velocity and concentration field type, *J. Geophys. Res.*, *114*, G02001, doi:10.1029/2008JG000710.
Faloona, I. (2009), Sulfur processing in the marine atmospheric boundary layer: A review and critical assessment of modeling uncertainties, *Atmos. Environ.*, *43*(18), 2841–2854.
Foster, A. F., M. A. Curran, B. T. Smith, T. D. van Ommen, and V. I. Morgan (2006), Covariation of sea ice and methanesulphonic acid in Wilhelm II Land, East Antarctica, *Ann. Glaciol.*, *44*, 429–432, doi:10.3189/172756406781811394.
Fundel, F., H. Fischer, R. Weller, F. Traufetter, H. Oerter, and H. Miller (2006), Influence of large-scale teleconnection patterns on methane sulfonate ice core records in Dronning Maud Land, *J. Geophys. Res.*, *111*, D04103, doi:10.1029/2005JD005872.
Gabric, A. J., J. M. Shephard, J. M. Knight, G. Jones, and A. J. Trevena (2005), Correlations between the satellite-derived seasonal cycles of phytoplankton biomass and aerosol optical depth in the Southern Ocean: Evidence for the influence of sea ice, *Global Biogeochem. Cycles*, *19*, GB4018, doi:10.1029/2005GB002546.
Gondwe, M., M. Krol, W. Klaassen, W. Gieskes, and H. de Baar (2004), Comparison of modeled versus measured MSA:nss $SO_4^=$ ratios: A global analysis, *Global Biogeochem. Cycles*, *18*, GB2006, doi:10.1029/2003GB002144.
Gosink, T. A., J. G. Pearson, and J. J. Kelley (1976), Gas movement through sea ice, *Nature*, *263*(5572), 41–42.
Holmes, C. D., D. J. Jacob, E. S. Corbitt, J. Mao, X. Yang, R. Talbot, and F. Slemr (2010), Global atmospheric model for mercury including oxidation by bromine atoms, *Atmos. Chem. Phys.*, *10*(24), 12,037–12,057.
Huebert, B. J., B. W. Blomquist, M. X. Yang, S. D. Archer, P. D. Nightingale, M. J. Yelland, J. Stephens, R. W. Pascal, and B. I. Moat (2010), Linearity of dms transfer coefficient with both friction velocity and wind speed in the moderate wind speed range, *Geophys. Res. Lett.*, *37*, L01605, doi:10.1029/2009GL041203.
IUPAC (2007), IUPAC Subcommittee for Gas Kinetic Data Evaluation data sheet sox76, report, [Available at http://www.iupac-kinetic.ch.cam.ac.uk/datasheets/pdf/SOx76_BrO_CH3SCH3.pdf], Cambridge Univ., Cambridge, U. K.
Jones, G., D. Fortescue, S. King, G. Williams, and S. Wright (2010), Dimethylsulphide and dimethylsulphoniopropionate in the south-west Indian Ocean sector of East Antarctica from 30° to 80°E during BROKE-West, *Deep Sea Res., Part II*, *57*(9–10), 863–876.
Karl, M., A. Gross, C. Leck, and L. Pirjola (2007), Intercomparison of dimethylsulfide oxidation mechanisms for the marine boundary layer: Gaseous and particulate sulfur constituents, *J. Geophys. Res.*, *112*, D15304, doi:10.1029/2006JD007914.
Kettle, A. J., and M. O. Andreae (2000), Flux of dimethylsulfide from the oceans: A comparison of updated data seas and flux models, *J. Geophys. Res.*, *105*(D22), 26,793–26,808.
Kettle, A. J., et al. (1999), A global database of sea surface dimethylsulfide (DMS) measurements and a procedure to predict sea surface DMS as a function of latitude, longitude, and month, *Global Biogeochem. Cycles*, *13*(2), 399–444.
Lana, A., et al. (2011), An updated climatology of surface dimethlysulfide concentrations and emission fluxes in the global ocean, *Global Biogeochem. Cycles*, *25*, GB1004, doi:10.1029/2010GB003850.
Legrand, M., and C. Feniet-Saigne (1991), Methanesulfonic-acid in South Polar snow layers—A record of strong El Nino?, *Geophys. Res. Lett.*, *18*(2), 187–190.
Levasseur, M., M. Gosselin, and S. Michaud (1994), A new source of dimethylsulfide (DMS) for the arctic atmosphere: Ice diatoms, *Mar. Biol.*, *121*(2), 381–387.
Liss, P., and L. Merlivat (1986), Air-sea gas exchange rates: Introduction and synthesis, in *The Role of Air-Sea Exchange in Geochemical Cycling*, edited by P. Buat-Menard, pp. 113–127, D Reidel, Norwell, Mass.
Liu, H. Y., D. J. Jacob, I. Bey, and R. M. Yantosca (2001), Constraints from ^{210}Pb and ^{7}Be on wet deposition and transport in a global three-dimensional chemical tracer model driven by assimilated meteorological fields, *J. Geophys. Res.*, *106*(D11), 12,109–12,128.
Loose, B., P. Schlosser, D. Perovich, D. Ringelberg, D. T. Ho, T. Takahashi, J. Richter-Menge, C. M. Reynolds, W. R. McGillis, and J. L. Tison (2011), Gas diffusion through columnar laboratory sea ice: Implications for mixed-layer ventilation of CO_2 in the seasonal ice zone, *Tellus, Ser. B*, *63*(1), 23–39.
Lucas, D. D., and R. G. Prinn (2005), Parametric sensitivity and uncertainty analysis of dimethylsulfide oxidation in the clear-sky remote marine boundary layer, *Atmos. Chem. Phys.*, *5*, 1505–1525.
Malin, G., and G. O. Kirst (1997), Algal production of dimethyl sulfide and its atmospheric role, *J. Phycol.*, *33*(6), 889–896.
Mayewski, P. A., et al. (2009), State of the Antarctic and Southern Ocean climate system, *Rev. Geophys.*, *47*, RG1003, doi: 10.1029/2007RG000231.
Minikin, A., M. Legrand, J. Hall, D. Wagenbach, C. Kleefeld, E. Wolff, E. C. Pasteur, and F. Ducroz (1998), Sulfur-containing species (sulfate and methanesulfonate) in coastal Antarctic aerosol and precipitation, *J. Geophys. Res.*, *103*(D9), 10,975–10,990.
Monaghan, A. J., et al. (2006), Insignificant change in antarctic snowfall since the International Geophysical Year, *Science*, *313*(5788), 827–831.
Nightingale, P. D., G. Malin, C. S. Law, A. J. Watson, P. S. Liss, M. I. Liddicoat, J. Boutin, and R. C. Upstill-Goddard (2000), In situ evaluation of air-sea gas exchange parameterizations using novel conservative and volatile tracers, *Global Biogeochem. Cycles*, *14*(1), 373–387.
Park, R. J., D. J. Jacob, B. D. Field, R. M. Yantosca, and M. Chin (2004), Natural and transboundary pollution influences on sulfate-nitrate-ammonium aerosols in the United States: Implications for policy, *J. Geophys. Res.*, *109*, D15204, doi:10.1029/2003JD004473.
Pasteur, E., R. Mulvaney, D. Peel, E. Saltzman, and P.-Y. Whung (1995), A 340 year record of biogenic sulphur from the Weddell Sea area, Antarctica, *Ann. Glaciol.*, *21*, 169–174.
Penner, J. E., et al. (2001), Aerosols, their direct and indirect effects, in *Climate Change 2001: The Scientific Basis. Contribution of Working Group I to the Third Assessment Report of the Intergovernmental Panel on Climate Change*, pp. 289–348, Cambridge Univ. Press, Cambridge, U. K.
Pham, M., J. F. Muller, G. P. Brasseur, C. Granier, and G. Megie (1995), A three-dimensional study of the tropospheric sulfur cycle, *J. Geophys. Res.*, *100*(D12), 26,061–26,092.
Preunkert, S., M. Legrand, B. Jourdain, C. Moulin, S. Belviso, N. Kasamatsu, M. Fukuchi, and T. Hirawake (2007), Interannual variability of dimethylsulfide in air and seawater and its atmospheric oxidation by-products (methanesulfonate and sulfate) at Dumont d'Urville, coastal Antarctica (1999–2003), *J. Geophys. Res.*, *112*, D06306, doi:10.1029/2006JD007585.
Preunkert, S., B. Jourdain, M. Legrand, R. Udisti, S. Becagli, and O. Cerri (2008), Seasonality of sulfur species (dimethyl sulfide, sulfate, and methanesulfonate) in Antarctica: Inland versus coastal regions, *J. Geophys. Res.*, *113*, D15302, doi:10.1029/2008JD009937.
Read, K. A., et al. (2008), DMS and MSA measurements in the Antarctic boundary layer: Impact of BrO on MSA production, *Atmos. Chem. Phys.*, *8*(11), 2985–2997.

Reynolds, R. W., N. A. Rayner, T. M. Smith, D. C. Stokes, and W. Q. Wang (2002), An improved in situ and satellite SST analysis for climate, *J. Clim.*, *15*(13), 1609–1625.

Saigne, C., and M. Legrand (1987), Measurements of methanesulfonic-acid in Antarctic ice, *Nature*, *330*(6145), 240–242.

Savoie, D. I., J. M. Prospero, R. J. Larsen, F. Huang, M. A. Izaguirre, T. Huang, T. H. Snowdon, L. Custals, and C. G. Sanderson (1993), Nitrogen and sulfur species in Antarctic aerosols at Mawson, Palmer Station, and Marsh (King George Island), *J. Atmos. Chem.*, *17*(2), 95–122.

Sciare, J., N. Mihalopoulos, and F. J. Dentener (2000), Interannual variability of atmospheric dimethylsulfide in the southern Indian Ocean, *J. Geophys. Res.*, *105*(D21), 26,369–26,377, doi:10.1029/2000JD900236.

Semiletov, I., A. Makshtas, S. I. Akasofu, and E. L. Andreas (2004), Atmospheric CO_2 balance: The role of Arctic sea ice, *Geophys. Res. Lett.*, *31*, L05121, doi:10.1029/2003GL017996.

Simó, R., and J. Dachs (2002), Global ocean emission of dimethylsulfide predicted from biogeophysical data, *Global Biogeochem. Cycles*, *16*(4), 1018, doi:10.1029/2001GB001829.

Simpson, W. R., D. Carlson, G. Honninger, T. A. Douglas, M. Sturm, D. Perovich, and U. Platt (2007), First-year sea-ice contact predicts bromine monoxide (BrO) levels at Barrow, Alaska better than potential frost flower contact, *Atmos. Chem. Phys.*, *7*, 621–627.

Spracklen, D. V., K. J. Pringle, K. S. Carslaw, M. P. Chipperfield, and G. W. Mann (2005), A global off-line model of size-resolved aerosol microphysics: I. Model development and prediction of aerosol properties, *Atmos. Chem. Phys.*, *5*, 2227–2252.

Sun, J. Y., J. W. Ren, and D. H. Qin (2002), 600 years record of biogenic sulfur from Lambert Glacier basin firn core, East Antarctica, *Ann. Glaciol.*, *35*, 362–367.

Tortell, P. D., and M. C. Long (2009), Spatial and temporal variability of biogenic gases during the Southern Ocean spring bloom, *Geophys. Res. Lett.*, *36*, L01603, doi:10.1029/2008GL035819.

von Glasow, R., and P. J. Crutzen (2004), Model study of multiphase dms oxidation with a focus on halogens, *Atmos. Chem. Phys.*, *4*, 589–608.

Wagner, T., O. Ibrahim, R. Sinreich, U. Friess, R. von Glasow, and U. Platt (2007), Enhanced tropospheric BrO over Antarctic sea ice in mid winter observed by MAX-DOAS on board the Research Vessel *Polarstern*, *Atmos. Chem. Phys.*, *7*(12), 3129–3142.

Wagnon, P., R. J. Delmas, and M. Legrand (1999), Loss of volatile acid species from upper firn layers at Vostok, Antarctica. *J. Geophys. Res.*, *104* (D3), 3423–3431.

Wang, Y. H., D. J. Jacob, and J. A. Logan (1998), Global simulation of tropospheric O_3-NO_x-hydrocarbon chemistry: 1. Model formulation, *J. Geophys. Res.*, *103*(D9), 10,713–10,725.

Wanninkhof, R. (1992), Relationship between wind-speed and gas-exchange over the ocean. *J. Geophys. Res.*, *97*(C5), 7373–7382.

Welch, K. A., P. A. Mayewski, and S. I. Whitlow (1993), Methanesulfonic-acid in coastal Antarctic snow related to sea-ice extent, *Geophys. Res. Lett.*, *20*(6), 443–446.

Weller, R., F. Traufetter, H. Fischer, H. Oerter, C. Piel, and H. Miller (2004), Postdepositional losses of methane sulfonate, nitrate, and chloride at the European Project for Ice Coring in Antarctica deep-drilling site in Dronning Maud Land, Antarctica, *J. Geophys. Res.*, *109*, D07301, doi:10.1029/2003JD004189.

Weller, R., D. Wagenbach, M. Legrand, C. Elsässer, X. Tian-Kunze, and G. König-Langlo (2011), Continuous 25-yr aerosol records at coastal Antarctica—I: Inter-annual variability of ionic compounds and links to climate indices, *Tellus, Ser. B*, *63*, 901–919, doi:10.1111/j.1600-0889.2011.00542.x.

Wesely, M. L. (1989), Parameterization of surface resistances to gaseous dry deposition in regional-scale numerical-models, *Atmos. Environ.*, *23*(6), 1293–1304.

Yang, X., R. A. Cox, N. J. Warwick, J. A. Pyle, G. D. Carver, F. M. O'Connor, and N. H. Savage (2005), Tropospheric bromine chemistry and its impacts on ozone: A model study, *J. Geophys. Res.*, *110*, D23311, doi:10.1029/2005JD006244.

Yuan, X. J., J. Patoux, and C. H. Li (2009), Satellite-based midlatitude cyclone statistics over the Southern Ocean: 2. Tracks and surface fluxes, *J. Geophys. Res.*, *114*, D04106, doi:10.1029/2008JD010874.

Zemmelink, H. J., J. W. H. Dacey, L. Houghton, E. J. Hintsa, and P. S. Liss (2008), Dimethylsulfide emissions over the multi-year ice of the western Weddell Sea, *Geophys. Res. Lett.*, *35*, L06603, doi:10.1029/2007GL031847.

Zwally, H. J., J. C. Comiso, C. L. Parkinson, D. J. Cavalieri, and P. Gloersen (2002), Variability of Antarctic sea ice 1979–1998, *J. Geophys. Res.*, *107*(C5), 3041, doi:10.1029/2000JC000733.

B. Alexander, C. M. Bitz, and P. J. Hezel, Department of Atmospheric Sciences, University of Washington, Box 351640, Seattle, WA 98195, USA. (phezel@atmos.washington.edu)

E. J. Steig, Department of Earth and Space Sciences, University of Washington, Box 351310, Seattle, WA 98195, USA.

C. D. Holmes, Department of Earth System Science, University of California, Irvine, 2101 Croul Hall, Irvine, CA 92697, USA.

J. Sciare, LSCI, CNRS-CEA-UVSQ, BAT 701, Orme des Merisiers, F-91191 Gif-sur-Yvette, France.

X. Yang, NCAS-Climate, Centre for Atmospheric Science, Department of Chemistry, University of Cambridge, Cambridge CB2 1EW, UK.